CrystEngComm

PAPER

View Article Online
View Journal | View Issue

Cite this: *CrystEngComm*, 2023, **25**, 6568

The odd–even effect in *n*-carboxyalkylammonium-containing organic–inorganic hybrids of Mn(II) halides: structural and magnetic characterisation†

Shalene N. Bothma, [a] Charles J. Sheppard, [b] Mark M. Turnbull, [c] Christopher P. Landee[d] and Melanie Rademeyer *[a]

The understanding of magnetic properties of hybrid compounds is important for the design of magnetic devices. In this contribution a prominent odd–even effect in both the structural characteristics and magnetic properties of four new hybrid compounds comprised of *n*-carboxyalkylammonium cations and perchloridomanganate anions is reported. When the *n*-carboxyalkylammonium cations contain an even number of carbon atoms, compounds of the formula $(NH_3(CH_2)_nCOOH)_2[MnCl_4]$, with n = 3 and 5, are formed, which display the two-dimensional (2D) hybrid halide perovskite structure in which bridging chlorido ligands link Mn^{2+} ions. Compounds containing *n*-carboxyalkylammonium cations with an odd number of carbon atoms have the formula $(NH_3(CH_2)_nCOOH)_2[MnCl_4(H_2O)_2]$, with n = 2 and 4, and display a zero-dimensional (0D) structure with hydrogen bonding interactions linking neighbouring $[MnCl_4(H_2O)_2]^{2-}$ anions. The odd–even effect is also evident in the magnetic properties of the compounds, which are linked to the structural differences observed in these compounds. Compounds containing an even number of carbon atoms show antiferromagnetic (AFM) interactions and spin canting at temperature T_N, with $2J_K$ = −8.28(5) K and T_N = 45.0(5) K when n = 3 and $2J_K$ = −7.72(4) K and T_N = 43(1) K when n = 5. Much weaker AFM interactions and no spin canting is observed in compounds containing an odd number of carbon atoms, with $2J_K$ = −0.14(2) K when n = 2 and $2J_K$ = −0.14(2) K when n = 4.

Received 29th August 2023,
Accepted 7th November 2023

DOI: 10.1039/d3ce00855j

rsc.li/crystengcomm

Introduction

In recent years, three-dimensional (3D) organic–inorganic hybrid halide perovskites of Pb^{2+} have been of interest because of their application in photovoltaic devices.[1–3] However, it has been shown that two-dimensional (2D) hybrid halide perovskites of Pb^{2+} offer certain advantages over their 3D counterparts.[4] 2D hybrid compounds containing metal ions other than Pb^{2+} often exhibit the 2D hybrid halide perovskite structure,[5] and these compounds also have interesting properties, with the resulting material typically combining the properties of the organic and inorganic components comprising the hybrid material.[5,6] Of specific interest in the current study are 2D hybrid halide perovskites containing the divalent metal ion Mn^{2+}, which imparts magnetic properties to the hybrid material.[7,8] Mn^{2+} has a low toxicity as well as low cost due to its natural abundance, making it a useful component for such materials.[9]

2D hybrid halide perovskites containing Mn^{2+} and *n*-alkylammonium or *n*-alkyldiammonium cations have been reported to exhibit interesting properties such as catalytic activity,[10] reversible barocaloric effects,[11] broadband emission for potential use in light emitting diodes,[12–14] potential use as solid–solid phase change materials[15] and ferroelastic properties.[16] Of specific interest in the current study, is the magnetic properties of these materials, with a number of reports on this topic in the literature.[17,18]

The magnetic properties exhibited by a material may be influenced by, among other things, the dimensionality of the structure, where structural dimensionality is determined by covalent or coordination bonding.[19] In the case of *n*-alkylammonium or *n*-alkyldiammonium-containing 2D hybrid halide perovskites of Mn^{2+}, a layered, 2D structure is typically formed, consisting of alternating organic and inorganic layers, making them low-dimensional magnetic materials.[20] The organic layers contain the organic cation, and the inorganic layers are comprised of corner sharing $[MX_6]^{4-}$ octahedra, with no Jahn–Teller distortion.[20] Mn^{2+} is a

[a] *Department of Chemistry, University of Pretoria, Pretoria, 0002, South Africa. E-mail: melanie.rademeyer@up.ac.za*
[b] *Cr Research Group, Department of Physics, University of Johannesburg, Auckland Park, Johannesburg, 2006, South Africa*
[c] *Carlson School of Chemistry and Biochemistry, Clark University, 950 Main St., Worcester, Massachusetts, 01610, USA*
[d] *Department of Physics, Clark University, 950 Main St., Worcester, Massachusetts, 01610, USA*

† Electronic supplementary information (ESI) available. CCDC 2281554–2281557. For ESI and crystallographic data in CIF or other electronic format see DOI: https://doi.org/10.1039/d3ce00855j

$S = 5/2$ ion,[21] and in the 2D hybrid halide perovskite structure the magnetic metal ions are linked by halido ligands to form approximately linear, symmetrical Mn–X–Mn bonds, with X = Cl^- or Br^-.[20] According to the Goodenough–Kanamori rules,[22,23] this linear magnetic superexchange is antiferromagnetic (AFM) in nature, resulting in compounds exhibiting quasi-2D AFM behaviour.[24,25]

A number of 2D Mn^{2+} hybrid chloride perovskites containing *n*-alkylammonium, *n*-alkyldiammonium or aryl-ammonium cations have been reported to show rich magnetic behaviour, including spin canting and spin–flop transitions.[26,27] The 2D perovskite $(CH_3NH_3)_2[MnCl_4]$ is a canted antiferromagnet below 47 K, and exhibits a spin–flop transition.[18,24,25,28] Canted antiferromagnetism has also been reported for the perovskite $(C_6H_5C_2H_4NH_3)_2[MnCl_4]$ below 44.3 K, attributed to a spin–flop transition.[29] The perovskite $(C_3H_7NH_3)_2[MnCl_4]$ was reported to exhibit spin canting.[27] A study of a series of compounds with the formula $(C_6H_5C_xH_{2x}NH_3)_2[MnCl_4]$, with $x = 0$ to 4, showed that all the compounds exhibit 2D antiferromagnetism, and spin canting below ordering temperatures ranging from 42–46 K.[30] In addition, work by Asensio *et al.*[26] showed that spin canting and a spin–flop transition are observed for the compounds $(C_6H_5CH_2CH_2NH_3)_2[MnCl]_4$ and $(C_2H_5NH_3)_2[MnCl]_4$, but no spin canting, and a weak spin–flop transition is observed for the compound $(NH_3C_2H_2NH_3)[MnCl]_4$. The authors attributed the difference in behaviour to the relative orientations of neighbouring inorganic layers of the compounds, because of the presence of either a mono-cation or a dication. Spin canting has also been observed in the 2D perovskite $(C_6H_5C_2H_3FNH_3)_2[MnCl]_4$.[31]

The spin canting observed in these Mn^{2+} perovskites is attributed to the tilting of the $[MnCl_6]^{4-}$ octahedra in the inorganic layer, since spin canting depends on the symmetry of the structure.[27,32] A weak net moment is present in the inorganic plane, due to the spin canting. There are two sources of spin canting in these types of compounds. The first is anisotropy, while the second occurs as a result of antisymmetric Dzyaloshinskii–Moriya exchange interactions, because of the tilted $[MnCl_6]^{4-}$ octahedra in the inorganic layer.[25] Single crystal studies showed anisotropy in the magnetisation of the in-plane and the out-of-plane directions.[26,28–30] In the these studies[26,28–30] the magnetic susceptibility was shown to approach zero with a decrease in temperature when measured out-of-plane, and it was shown to increase when measured in-plane, indicating that the easy-axis lies perpendicular to the inorganic plane.

In the current study, the structural characteristics and magnetic properties of compounds formed through the combination of $MnCl_2$ and *n*-carboxyalkylamines $(NH_2(CH_2)_nCOOH)$ in the presence of HCl have been investigated. The *n*-carboxyalkylammonium cation, $(NH_3(CH_2)_nCOOH)^+$, that is formed through the protonation of a *n*-carboxyalkylamine molecule by an acid, is related to *n*-alkylammonium and *n*-alkyldiammonium cations since it also contains a terminal ammonium group and an alkyl portion, and it has a similar linear shape. However, the *n*-carboxyalkylammonium cation differs in terms of its hydrogen bonding capability compared to that of an *n*-alkylammonium or *n*-alkyldiammonium cation.[8,33,34] An *n*-alkylammonium cation has only one hydrogen bond donor group in the form of a single terminal ammonium group, while the *n*-alkyldiammonium cation has two hydrogen bonding terminal ammonium groups. In the *n*-carboxyalkylammonium cation, both a terminal ammonium group, which can act as a hydrogen bonding donor, as well as a terminal carboxylic acid group, are present. The terminal carboxylic acid group can act as both a hydrogen bond donor or acceptor, thus, two hydrogen bonding donors (the ammonium group and the carboxylic acid group), and one hydrogen bonding acceptor (the carboxylic acid group) are present in an *n*-carboxyalkylammonium cation, while the *n*-alkylammonium and *n*-alkyldiammonium cations only contain hydrogen bonding donor groups. *n*-Carboxyalkylammonium cations may form supramolecular dimers that mimic long chain *n*-alkyldiammonium cations.[33]

Of specific interest is the type of structure formed for perchloridomanganate hybrid compounds containing *n*-carboxyalkylammonium cations, and whether these compounds exhibit the 2D hybrid halide perovskite structure like their *n*-alkylammonium or *n*-alkyldiammonium counterparts, or not. Moreover, the effect of the number of carbon atoms in the *n*-carboxyalkylammonium cation on the type of structure formed, as well as on the magnetic behaviour of the compound, is of interest, since an odd–even structural effect is often observed in compounds containing alkyl chains.[35–38]

A search of the Cambridge Structural Database (CSD) (Version 5.43, June 2022 update)[39] showed that no structures of compounds comprised of *n*-carboxyalkylammonium cations and perchloridomanganate anions have been reported in the literature to date, hence the focus of the current study on the investigation of the structural aspects and magnetic properties of these materials.

The *n*-carboxyalkylammonium compounds and their structures will be abbreviated as **C*x*MnCl**, where *x* indicates the number of carbon atoms in the *n*-carboxyalkylammonium cation. For example, when the cation is 2-carboxyethylammonium, $(NH_3(CH_2)_2COOH)^+$, $x = 3$. In the case where aqua ligands are present, the abbreviation **C*x*MnClH_2O** will be used.

Experimental

Chemicals and reagents

All chemicals were used as purchased without further purification: $MnCl_2{\cdot}4H_2O$ (Sigma-Aldrich, ≥99%), 3-aminopropanoic acid (Sigma-Aldrich, 99%), 4-aminobutyric acid (Sigma, 99%), 5-aminopentanoic acid (Sigma-Aldrich, 99%), 6-aminohexanoic

acid (Sigma-Aldrich, ≥99%), HCl (Sigma-Aldrich, 37%) and chloroform (Sigma-Aldrich, ≥99.8%).

Synthesis

All reactions followed a similar synthetic procedure carried out in excess HCl with a stoichiometric L : $MnCl_2$ ratio of 2 : 1, where L indicates the *n*-carboxyalkylamine. Good quality single crystals were harvested from the reaction vessels and washed using chloroform. No attempt was made to optimise the yields of the reactions.

Synthesis of bis-(2-carboxyethylammonium) diaquatetrachloridomanganate(II), C3MnClH$_2$O. 3-Aminopropanoic acid (0.5348 g, 6.000 mmol) and $MnCl_2{\cdot}4H_2O$ (0.5938 g, 3.000 mmol) were added to 1 ml 37% HCl in a size six vial. The vial was closed and then sealed with Parafilm. The sealed vial was placed in an oil bath that was heated to 70 °C. As the solution was heated, the reagents dissolved over time to produce a clear solution. Once the reagents were completely dissolved, the oil bath was switched off and allowed to cool to room temperature. At room temperature it was observed that light pink block shaped crystals formed in the vial with the mother liquor. These were isolated from the mother liquor and washed with chloroform. Elemental analysis: calculated: C: 17.34%, H: 4.92%, N: 7.08%; experimental: C: 17.45%, H: 4.88%, N: 6.78%. Percentage yield: 15.25%. Mass yield: 0.19 g. This reaction was reproducible with the same product forming from many repetitions of the reaction.

Synthesis of bis-(3-carboxypropylammonium) tetrachloridomanganate(II), C4MnCl. 4-Aminobutanoic acid (0.5326 g, 5.979 mmol) and $MnCl_2{\cdot}4H_2O$ (0.5937 g, 2.999 mmol) were added to 1 ml 37% HCl in a size six vial. The vial was closed with a lid and sealed with Parafilm. The sealed vial was placed in an oil bath at 70 °C. As the solution was heated, the reagents dissolved over time to produce a clear solution. Once the reagents were completely dissolved, the oil bath was switched off to allow cooling of the solution to room temperature. Upon cooling of the solution, colourless plate-shaped crystals formed, which were isolated from the mother liquor, and washed with chloroform. Elemental analysis: calculated: C: 12.82%, H: 2.88%, N: 5.26%; experimental: C: 12.79%, H: 2.86%, N: 4.97%. Percentage yield: 24.28%. Mass yield: 0.30 g. This reaction was reproducible with the same product forming from many repetitions of the reaction.

Synthesis of bis-(4-carboxybutylammonium) diaquatetrachloridomanganate(II), C5MnClH$_2$O. 5-Aminopentanoic acid (0.6180 g, 5.993 mmol) and $MnCl_2{\cdot}4H_2O$ (0.5940 g, 3.001 mmol) were added to 1 ml 37% HCl in a size 6 vial. The vial was closed with a lid and sealed with Parafilm. The sealed vial was placed in an oil bath at 70 °C. As the solution was heated, the reagents dissolved to produce a clear solution, after which the oil bath was switched off to allow cooling of the solution to room temperature. Upon cooling of the solution, light pink block shaped crystals formed, and these crystals were harvested from the mother liquor, and washed with chloroform. Elemental analysis: calculated: C: 23.23%, H: 4.87%, N: 6.77%; experimental: C: 23.21%, H: 4.74%, N: 7.00%. Percentage yield: 26.78%. Mass yield: 0.38 g. This reaction was reproducible with the same product forming from many repetitions of the reaction.

Synthesis of bis-(5-carboxypentylammonium) tetrachloridomanganate(II), C6MnCl. 6-Aminohexanoic acid (0.7861 g, 5.998 mmol) and $MnCl_2{\cdot}4H_2O$ (0.5942 g, 3.002 mmol) were added to 1 ml 37% HCl in a size 6 vial. The vial was closed with a lid and sealed with Parafilm. The sealed vial was placed in an oil bath at 70 °C. Heating of the solution resulted in the reagents dissolving over time to produce a clear solution. Once the reagents were completely dissolved, the oil bath was switched off to allow cooling of the solution to room temperature. Upon cooling of the solution, light pink plate-shaped crystals formed, and the crystals were isolated from the mother liquor and washed with chloroform. Elemental analysis: calculated: C: 16.25%, H: 3.41%, N: 4.74%; experimental: C: 16.38%, H: 3.48%, N: 4.85%. Percentage yield: 29.55%. Mass yield: 0.41 g. This reaction was reproducible with the same product forming from many repetitions of the reaction.

Instrumental studies

Single crystal X-ray diffraction. Single crystal X-ray diffraction data for structures **C3MnClH$_2$O**, **C4MnCl** and **C5MnClH$_2$O** were collected at 150 K on a Bruker D8 Venture diffractometer, with a Photon 100 CMOS detector, employing a combination of ϕ and ω scans. Monochromatic Mo-Kα radiation of wavelength 0.71073 Å from an Incotec Microfocus Source ($I\mu$s) was employed as irradiation source. Sample cooling was achieved using an Oxford Cryogenics Cryostat. Data reduction were performed using the software SAINT+[40] and absorption corrections were performed using SADABS[41] as part of the APEXII suite.[42]

Single crystal X-ray diffraction data for the **C6MnCl** structure were collected on a Rigaku XtaLAB Synergy R diffractometer, with a HyPix CCD detector, at 150 K, using ω scans and a rotating-anode X-ray source supplying monochromatic Mo-Kα radiation of wavelength 0.71073 Å. Cooling was achieved using an Oxford Cryogenics Cryostat. Data reduction and absorption corrections were carried out using the CrysAlisPro (Version 1.171.40.23a) software package.[43]

All the crystal structures were solved either by direct methods or intrinsic phasing using SHELX-2014/7[44] as part of the WinGX suite.[45] Structure refinements were done using SHELXL[46] in WinGX[45] as GUI. Graphics and publication material were generated using Mercury 2022.2.0.[47]

All non-hydrogen atoms for all structures were refined anisotropically. In structures **C3MnClH$_2$O** and **C4MnCl** the hydrogen atom on the carboxylic acid group was placed as

observed in the difference map, and its position refined, while the rest of the hydrogen atoms were placed in calculated positions and allowed to ride on the parent atoms. In structure **C5MnClH$_2$O** the hydrogen atoms on the carbon atoms were placed in calculated positions and allowed to ride on the parent atoms, while the rest were all placed as observed in the difference map and their positions refined. One of the hydrogen atoms on one carboxylic acid group of structure **C6MnCl** was placed as observed in the difference map and its position refined, while the rest of the hydrogen atoms were placed in calculated positions and allowed to ride on the parent atoms.

Powder X-ray diffraction. Samples used for powder X-ray diffraction were ground to a fine, polycrystalline powder, employing an agate mortar and pestle. Powder X-ray diffraction patterns were collected on a Bruker D2 Phaser powder diffractometer at room temperature, employing a Si low-background sample holder. The powder diffraction patterns were measured over a 2θ range of 5° to 40° 2θ, at 2 seconds/0.05° increments employing Cu-Kα radiation at a wavelength of 1.5406 Å. Experimental powder patterns were compared with powder diffraction patterns calculated from single crystal structure data using the software DiffractWD.[48] A comparison of the measured and calculated powder patterns is shown in the ESI† Section S1.

Magnetic analysis. Magnetic data for all the compounds were measured using a Quantum Design MPMS-XL SQUID magnetometer. Powdered samples were placed in a gelatin capsule mounted in a plastic straw. Magnetisation was measured at 1.8 K as a function of applied field from 0–50 kOe. Several data points were recollected as the field was returned to zero to monitor for hysteresis effect; none were observed. Magnetisation was then collected as a function of temperature from 1.8 K to 310 K in a 1 kOe applied field. The measured data were corrected for diamagnetic contributions from the atoms comprising the compounds using Pascal's constants[49] and for the background of an empty gelatin capsule and straw (measured independently).

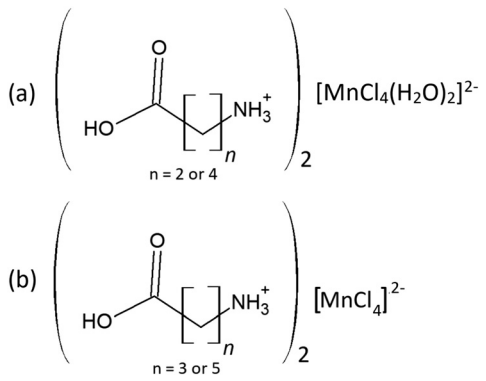

Scheme 1 Compounds structurally characterised in this study. (a) 0D organic–inorganic hybrids. (b) 2D hybrid halide perovskites.

Results and discussion

Crystallographic discussion of structures

In this study two types of structures were determined, as illustrated in Scheme 1. Firstly the structures of two bis-(*n*-carboxyalkylammonium)diaquatetrachloridomanganate compounds of the formula $(NH_3(CH_2)_nCOOH)_2[MnCl_4(H_2O)_2]$, with n = 2 and 4, abbreviated **C3MnClH$_2$O** and **C5MnClH$_2$O** were determined. In addition, the structures of two bis-(*n*-carboxyalkylammonium)tetrachloridomanganate compounds of the formula $(NH_3(CH_2)_nCOOH)_2[MnCl_4]$, with n = 3 and 5, abbreviated **C4MnCl** and **C6MnCl**, were determined.

The crystallographic parameters are listed in Table 1, the asymmetric units are shown in Fig. 1, and selected bond lengths, angles, torsion angles, hydrogen bonding parameters and other structural descriptors are listed in Table 2.

Structural descriptors. Two structures determined in this study can be classified as 2D hybrid halide perovskites, namely structures **C4MnCl** and **C6MnCl**, and two structures, **C3MnClH$_2$O** and **C5MnClH$_2$O**, are categorised as 0D hybrid complexes. A number of structural descriptors will be employed to compare certain geometric features of these structures, as used by other authors in the literature,[9] or adapted where required, with each structural descriptor relevant to a specific structural characteristic. The geometric descriptors are illustrated in Fig. 2. These include the polyhedra tilt descriptors (the ψ angle and Mn–Cl–Mn bridging angle), and the cation geometric descriptors (the β and ϕ angles). The descriptors are described in more detail below.

Polyhedra tilt angles (ψ) and Mn–Cl–Mn bridging angle. The descriptor ψ is the angle formed between the equatorial plane about the Mn^{2+} ion and the inorganic plane, as defined by the mean plane through the metal ions of a single inorganic layer. ψ indicates the tilt of the polyhedra, as illustrated in Fig. 2(a), and is applicable to all structure types, as all polyhedra may display a polyhedral tilt angle.

The Mn–Cl–Mn bridging angle describes the rotational tilt of the polyhedra about the plane perpendicular to the inorganic plane, as illustrated in Fig. 2(b). The Mn–Cl–Mn bridging angle is applicable only to the 2D hybrid halide perovskite structures and not the 0D hybrid structures, as no bridging halido ligands are present between neighbouring metal ions in the 0D structures.

Cationic tilt angles (β and ϕ). To describe the placement of the ammonium group relative to the inorganic plane, and the orientation of an individual cation, the descriptors β and ϕ will be employed. The inorganic plane is defined as previously described.

The β angle indicates the angle between the C–N bond and the inorganic plane, as shown in Fig. 2(c). This geometric parameter is used for both the 2D and 0D structures. The angle ϕ is defined as the angle formed between the inorganic plane and the vector connecting the carbon atom bonded to the nitrogen atom and the carboxy carbon atom, as shown in Fig. 2(d). Thus, the ϕ angle gives

Table 1 Crystallographic parameters

Abbreviation	C3MnClH$_2$O	C4MnCl	C5MnClH$_2$O	C6MnCl
Empirical formula	$(C_3H_8O_2N^+)_2[MnCl_4(H_2O)_2]^{2-}$	$(C_4H_{10}O_2N^+)_2[MnCl_4]^{2-}$	$(C_5H_{12}O_2N^+)_2[MnCl_4(H_2O)_2]^{2-}$	$(C_6H_{14}O_2N^+)_2[MnCl_4]^{2-}$
Formula weight (g mol^{-1})	412.98	405.00	469.08	461.10
Temperature (K)	150(2)	150(2)	150(2)	150(2)
Wavelength (Å)	0.71073	0.71073	0.71073	0.71073
Crystal system	Monoclinic	Monoclinic	Triclinic	Triclinic
Space group	*C*2/*c*	$P2_1/c$	$P\bar{1}$	$P\bar{1}$
a (Å)	21.3208(14)	16.1956(4)	5.9046(4)	7.1370(1)
b (Å)	7.0794(4)	7.1780(6)	7.8188(5)	7.2664(1)
c (Å)	11.1440(6)	7.2126(6)	11.5638(7)	19.6318(4)
α (°)	90	90	91.740(2)	85.695(2)
β (°)	107.916(2)	100.097(2)	99.872(2)	87.366(2)
γ (°)	90	90	104.651(2)	88.660(2)
Volume (Å^3)	1600.49(16)	825.49(4)	507.33(6)	1013.96(3)
Z	4	2	1	2
Density calculated (g cm^{-3})	1.714	1.629	1.535	1.510
Absorption coefficient (mm^{-1})	1.511	1.455	1.202	1.195
F(000)	844	414	243	478
Crystal size (mm^3)	0.265 × 0.326 × 0.606	0.050 × 0.104 × 0.232	0.021 × 0.263 × 0.347	0.053 × 0.121 × 0.263
Reflections collected	19 734	15 457	14 955	29 420
Unique reflections	1665 [$R_{(int)}$ = 0.0334]	2239 [$R_{(int)}$ = 0.0268]	2113 [$R_{(int)}$ = 0.0302]	4138 [$R_{(int)}$ = 0.0315]
Completeness	99.9	99.9	99.9	99.9
Data/restraints/parameters	1665/1/125	2239/0/93	2114/0/130	4138/0/214
Goodness-of-fit F^2	1.160	1.129	1.077	1.110
Final *R* indices [$I > 2\sigma(I)$]	R_1 = 0.0182	R_1 = 0.0199	R_1 = 0.0192	R_1 = 0.0256
	wR_2 = 0.0458	wR_2 = 0.0502	wR_2 = 0.0459	wR_2 = 0.0616
R indices (all data)	R_1 = 0.0206	R_1 = 0.0220	R_1 = 0.0233	R_1 = 0.0288
	wR_2 = 0.0467	wR_2 = 0.0512	wR_2 = 0.0476	wR_2 = 0.0626

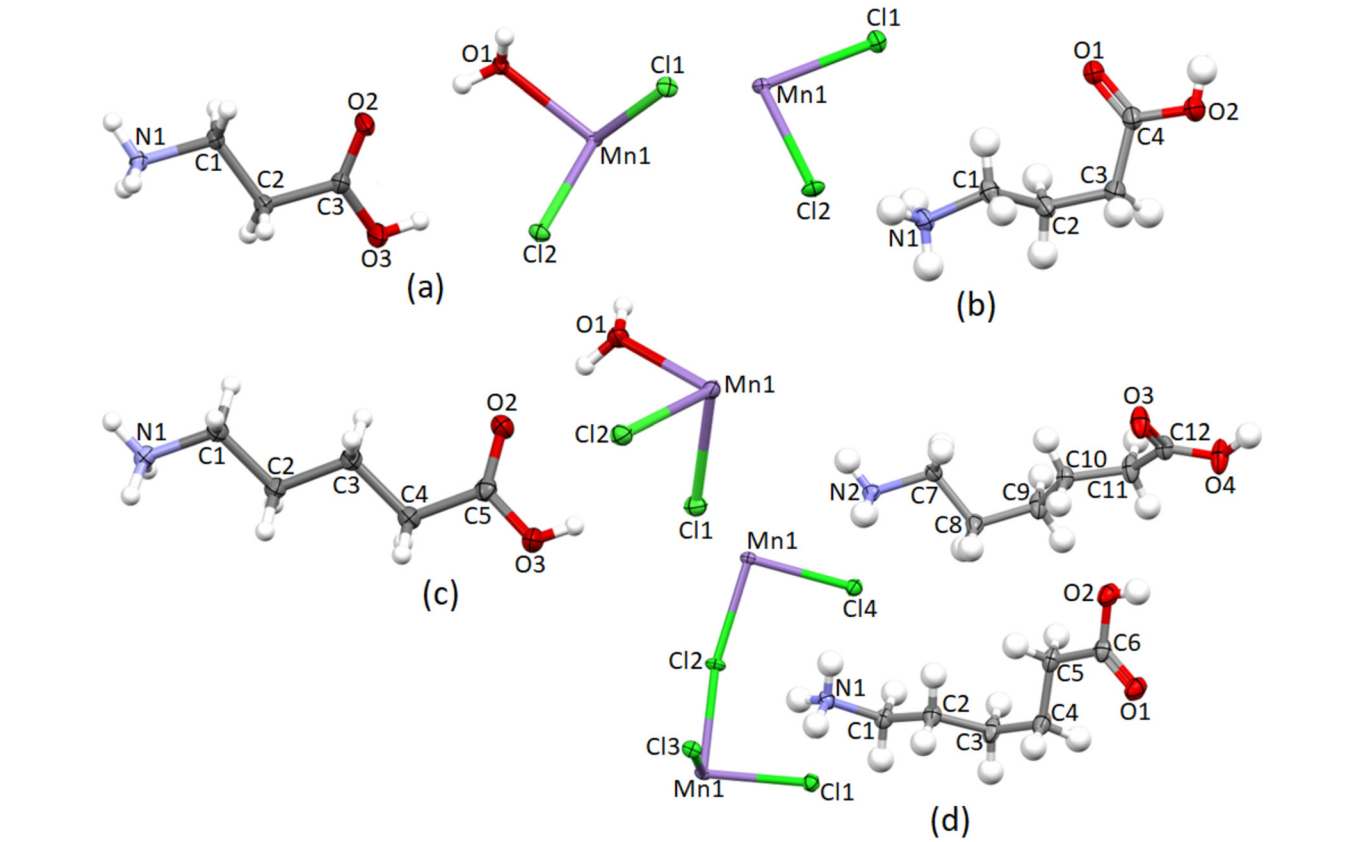

Fig. 1 The asymmetric units, with atomic numbering schemes for structures (a) **C3MnClH$_2$O**, (b) **C4MnCl**, (c) **C5MnClH$_2$O**, and (d) **C6MnCl**. The ellipsoids are drawn at the 50% probability level. The hydrogen atoms are drawn as spheres of arbitrary radii.

Table 2 Geometric parameters, structural descriptors, and hydrogen bonding interactions

Structure	C3MnClH$_2$O	C4MnCl	C5MnClH$_2$O	C6MnCl
Perovskite layer orientation	Staggered	Staggered	Staggered	Staggered
M–Cl bond length (Å)	2.4732(4) 2.5656(4)	2.5571(3) 2.4853(3) 2.5632(3)	2.5034(4) 2.5672(4)	2.4920(4) 2.5040(4) 2.5419(4) 2.6025(4) 2.5903(4) 2.5376(4)
M–O bond length (Å)	2.2248(9)	—	2.1872(11)	—
M⋯M distance (Å)	5.572	5.088	5.905	5.033 5.152
Area of interstitials (Å^2)	—	25.89	—	25.93
Penetration depth (Å)	—	0.153	—	0.168
Mn–Cl⋯Cl–Mn contact distance (Å)	6.990	11.005	8.327	14.614
Layer repeat distance (Å)	10.143	15.945	11.358	19.557
Supramolecular cation length (Å)	—	12.189	—	17.211 17.412
Mn–Cl⋯Cl–Mn bridging angle (°)	—	167.097(13)	—	164.430(2) 165.590(2)
ψ angle (°)	46.83	7.43	46.31	7.63 7.59
β angle (°)	83.22	78.71	88.28	69.28 63.74
ϕ angle (°)	62.80	84.78	76.64	68.02 68.42
N–C–C–C torsion angle (°) (*gauche* bond)	174.58(11)	—	−173.10(12)	—
C–C–C–C torsion angle (°) (*gauche* bond)	—	−73.24(18)	—	−66.27(7) 70.41(7)
Hydrogen bonding configuration	—	t^2b	—	t^2b
N–H$^+$⋯$^-$Cl–Mn (D⋯A) distance (Å)	3.1742(12)^{i} 3.3211(12)^{ii}	3.1973(11)^{vi} 3.2748(11) 3.4484(11)^{vii} 3.4710(12)^{viii}	3.1612(13)^{x} 3.2178(13)^{x} 3.3033(13)^{xi} 3.4316(14)^{v}	3.2473(16) 3.2512(17)^{xiii} 3.2679(18) 3.2705(17)^{xiv} 3.2978(18) 3.3973(17)^{xv} 3.2506(17)^{v}
N–H$^+$⋯O$_{(aqua)}$–Mn (D⋯A) distance (Å)	2.9677(15)^{iii}	—	3.1396(11)^{x}	—
C–O–H⋯$^-$Cl–Mn (D⋯A) distance (Å)	3.1003(11)^{iv}	—	3.0835(12)	—
Mn–O–H$_{(aqua)}$⋯$^-$Cl–Mn (D⋯A) distance (Å)	3.1666(10)^{v}	—	3.1799(11)^{xii}	—
Mn–O–H⋯O═C (D⋯A) distance (Å)	2.7335(14)	—	2.7486(15)	—
O–H⋯O═C (D⋯A) distance (Å)	—	2.6330(14)^{v}	—	2.615(2)^{xvi} 2.639(2)

Symmetry operators for hydrogen bonding acceptors: i: $-x+\frac{1}{2}, y-\frac{1}{2}, -z+\frac{1}{2}$; ii: $x-\frac{1}{2}, y-\frac{1}{2}, z$; iii: $-x+\frac{1}{2}, y+\frac{1}{2}, -z+\frac{1}{2}$; iv: $-x+1, -y+1, -z+1$; v: $-x+1, y, -z+\frac{1}{2}$; vi: $x, -y+3/2, z-\frac{1}{2}$; vii: $x, -y+\frac{1}{2}, z-\frac{1}{2}$; viii: $x, y, z-1$; ix: $-x+2, -y+2, -z+1$; x: $-x+1, -y+2, -z+1$; xi: $x, y, z+1$; xii: $x-1, y, z$; xiii: $x+1, y, z$; xiv: $-x+1, -y+1, -z+2$; xv: $-x, -y+2, -z+2$; xvi: $-x+2, -y, -z+1$.

an average tilt of a single cation relative to the inorganic plane. A ϕ angle close to 90° is indicative of cations that pack approximately perpendicular to the inorganic plane. The ϕ angle is used as geometric parameter in both 2D and 0D structures.

Layer repeat distance and inter-layer Mn–Cl$^-$⋯$^-$Cl–Mn or Mn–O⋯O–Mn contact distance. Both types of structures determined in this study form layered assemblies, thus, the layer repeat distance and inter-layer Mn–Cl$^-$⋯$^-$Cl–Mn or Mn–O⋯O–Mn contact distances can be determined.

The layer repeat distance refers to the distance between two neighbouring inorganic planes, as defined by the perpendicular distance between the mean planes through the metal ions of consecutive inorganic layers. The inter-layer Mn–Cl$^-$⋯$^-$Cl–Mn contact distance indicates the shortest distance between two terminal halido ligands in consecutive inorganic sheets in the 2D hybrid halide perovskite structures. The Mn–O⋯O–Mn contact distance refers to the shortest distance between two oxygen atoms of aqua ligands coordinated to metal ions in neighbouring inorganic layers in 0D hybrid structures.

Eclipsed and staggered inorganic perovskite layers. Single layer 2D oxide perovskites can be categorised as either Ruddlesden–Popper (RP)[50] or Dion–Jacobson (DJ)[51] perovskites. RP and DJ structures of oxide perovskites differ in terms of the relative orientation of neighbouring inorganic layers. For the DJ structures, neighbouring perovskite metal oxide layers are eclipsed, with an offset of (0,0) or ($\frac{1}{2}$,0) of one of the M⋯M distances, relative to each other, while for the RP structures neighbouring layers are staggered, with an

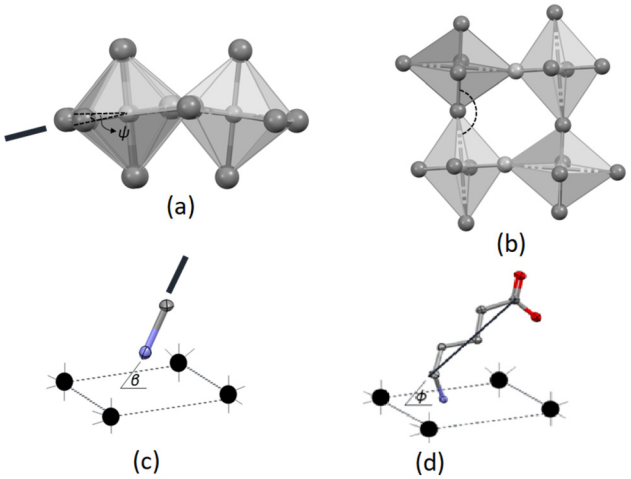

Fig. 2 Illustration of structural descriptors: (a) ψ angle (b) Mn–Cl–Mn bridging angle indicated by black dashed lines (c) β angle and (d) ϕ angle.

offset of $(\frac{1}{2},\frac{1}{2})$ of the M⋯M distance. Typically, RP structures are associated with 2D perovskites containing monocations, thus the formula of a RP structure is usually A_2MO_4, where A is a monocation. DJ structures normally form when 2D perovskites contain dications, thus typically of the formula A′MO_4, where A′ is a dication.[51,52] The same classification has been employed for 2D layered hybrid halide perovskite structures. However, due to the increased size and flexibility of the organic cation in 2D layered hybrid halide perovskites, as well as possible non-covalent interactions between cations or between cations and the inorganic layer, exceptions may occur, and 2D hybrid halide perovskite structures have been shown to have inorganic layers orientated between the two extremes of DJ and RJ, shown in Fig. 3(a) and (b), respectively.[52] Tremblay *et al.*[52] defined the term "near-DJ" (nDJ) when the offset is close to, but not exactly (0,0) or $(\frac{1}{2},0)$ (in either direction), for example, see Fig. 3(c), and "near-RP" (nRP) when the offset is close to, but not exactly $(\frac{1}{2},\frac{1}{2})$, see, for example Fig. 3(d). This classification will be employed in the current study to classify the 2D hybrid halide perovskite structures according to the relative orientation of their consecutive inorganic layers.[51,52]

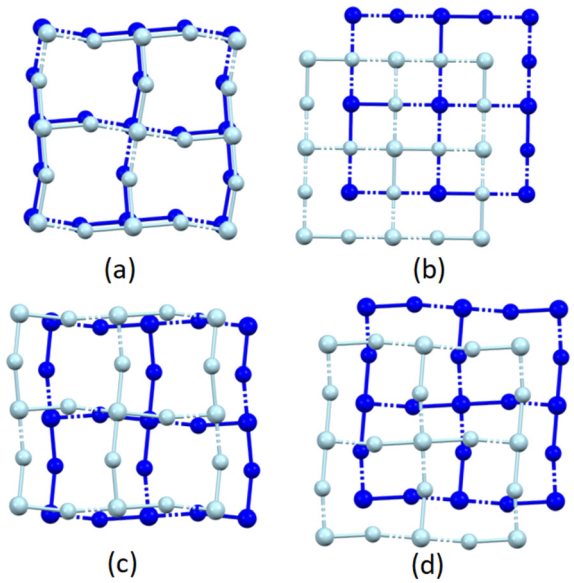

Fig. 3 Relative orientation of consecutive inorganic layers in (a) an ideal Dion–Jacobson (DJ) structure (b) an ideal Ruddlesden–Popper (RP) structure (c) a near Dion–Jacobson (nDJ) structure and (d) a near Ruddlesden–Popper (nRP) structure.

Ammonium group hydrogen bonding geometries. In 2D hybrid halide perovskite structures, the positioning of the ammonium group relative to the inorganic layer through hydrogen bonding is directional and this group is positioned to optimise hydrogen bonding interactions with the inorganic layer.

Based on the hydrogen atom geometries put forth by Mitzi,[53] the hydrogen atom configurations can be described as either bridging (b) or terminal (t), as shown in Fig. 4(a) and (b). Only the strong hydrogen bonding interactions, namely charge assisted N–$H^+\cdots^-$X–M interactions, are considered when determining the hydrogen bonding configuration, and when bifurcated or trifurcated interactions are present, the shortest N–$H^+\cdots^-$X–M interaction is considered. The nomenclature $b^m t^n$, $m + n = 3$,[53] is adopted, which describes the number of bridging (m) and terminal (n) halido ligand acceptors per hydrogen bonding configuration. Where more than three hydrogen bonding interactions are present, only the three shortest D⋯A hydrogen bond distances are considered. If the number of bridging hydrogen bonding acceptors outnumber terminal hydrogen bonding acceptors, the overall configuration is bridging, and the reverse is true if there are more terminal hydrogen bonding acceptors.

Structural results

The main structural features of the four structures are discussed below, with additional information on the structures included in ESI† Section S2.

C3MnClH$_2$O. The structure **C3MnClH$_2$O** crystallises in the monoclinic space group $C2/c$ and forms a 0D hybrid structure, with isolated organic cations and inorganic anions comprising the structure.[19] The asymmetric unit comprises one 2-carboxyethylammonium cation and a $[MnCl_2(H_2O)]^-$

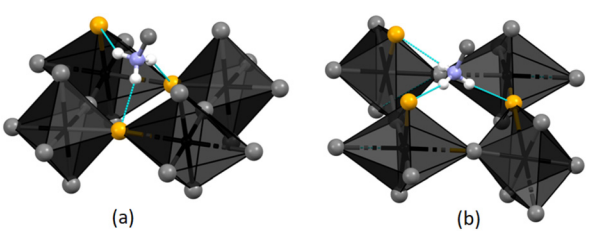

Fig. 4 (a) The bridging hydrogen bonding configuration. (b) The terminal hydrogen bonding configuration.

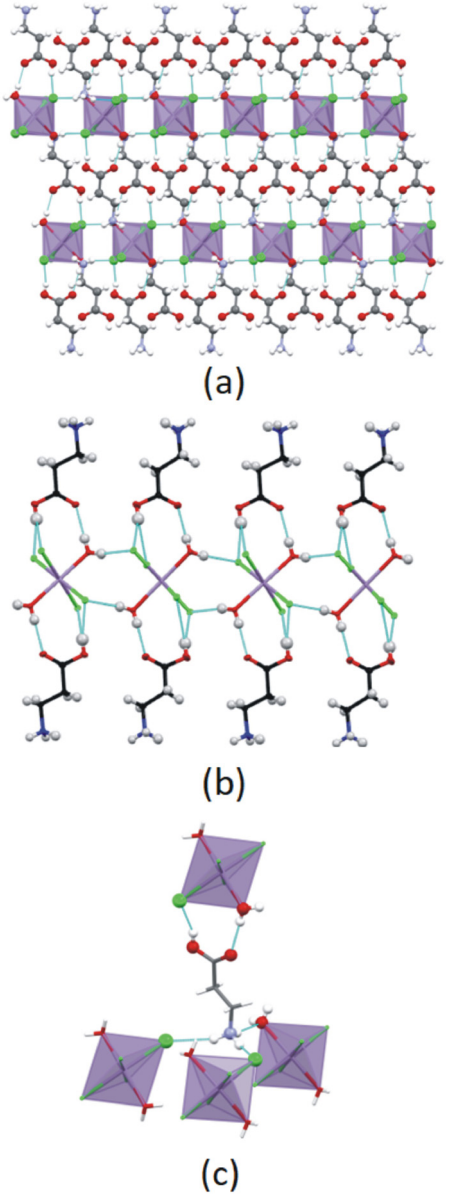

Fig. 5 (a) Packing diagram and hydrogen bonding network in structure **C3MnClH$_2$O**, as viewed down the *b*-axis. Hydrogen bonds are shown as blue dashed lines. (b) 1D hydrogen bonded ribbon formed along the *c*-direction in structure **C3MnClH$_2$O**. (c) Different types of hydrogen bonding interactions in structure **C3MnClH$_2$O**. Atoms involved in hydrogen bonding are indicated in ball representation while the rest of the atoms are shown in stick representation.

anionic unit, as shown in Fig. 1. The metal ion lies on an inversion centre, which generates the full $[MnCl_4(H_2O)_2]^{2-}$ anion. In this octahedral anion, four chlorido ligands and two aqua ligands are coordinated *trans* to each other to the metal ion.

The cation exhibits an all-*trans* conformation. A layered structure is formed, which is comprised of alternating organic and inorganic layers, as illustrated in Fig. 5(a). The organic layer is formed by interdigitated 2-carboxyethylammonium cations, while isolated $[MnCl_4(H_2O)_2]^{2-}$ anions comprise the inorganic layer. Adjacent inorganic layers adopt a staggered arrangement, whereby neighbouring inter-layer metal ions are off-set. The layer repeat distance is 10.143 Å and the Mn–O···O–Mn inter-layer distance is 7.873 Å.

Different types of hydrogen bonding interactions form a 3D hydrogen bonded network, as illustrated in Fig. 5(b). These include N–H$^+$···$^-$Cl–Mn, C–O–H···$^-$Cl–Mn, Mn–O–H···$^-$Cl–Mn, N–H$^+$···O–Mn, and Mn–O–H···O=C hydrogen bonding interactions.

In the inorganic layer, individual $[MnCl_4(H_2O)_2]^{2-}$ anions are cross-linked through Mn–O–H···$^-$Cl–Mn hydrogen bonding interactions to form 1D hydrogen bonded anionic ribbons, as shown in Fig. 5(b). The ψ angle is 46.83°, indicating that the polyhedra are tilted. The ammonium group and carboxylic acid group of a cation are hydrogen bonded to different inorganic layers with the chlorido and aqua ligands of the anions acting as hydrogen bonding acceptors, and the ammonium groups and carboxylic acid groups of the cations as hydrogen bond donors.

Cations hydrogen bond to both sides of the anionic hydrogen bonded ribbon through their carboxylic acid groups, as illustrated in Fig. 5(b), with the carboxylic acid groups acting as hydrogen bonding donors to chlorido ligands, while they accept hydrogen bonds from aqua ligands, to form a flat ribbon extending along the *c*-direction. Neighbouring ribbons are further linked by hydrogen bonding ammonium groups, with each ammonium group forming two classical, charge assisted N–H$^+$···$^-$Cl–Mn hydrogen bonds to one ribbon, as well as a classical, charge-assisted N–H$^+$···$^-$Cl–Mn hydrogen bond to a neighbouring ribbon, thereby linking the ribbons. The β angle of the ammonium group is 84.89° and the ϕ angle is 62.80°.

C5MnClH$_2$O. The structure **C5MnClH$_2$O** crystallises in the triclinic space group $P\bar{1}$, and forms a 0D hybrid structure, with isolated organic cations and inorganic anions comprising the structure.[19] The asymmetric unit, as illustrated in Fig. 1, comprises one 4-carboxybutylammonium cation and one $[MnCl_2(H_2O)]^-$ moiety, with the metal ion located on an inversion centre, which generates the rest of the $[MnCl_4(H_2O)_2]^{2-}$ anion.

The 4-carboxybutylammonium cation adopts the all-*trans* conformation, with all torsion angles close to 180°. The β angle equals 88.28°, indicating the tilting of the cations relative to the inorganic plane and the ϕ angle is 76.64°.

The ψ angle is 46.31°, and is indicative of the tilt of the octahedra.

Packing of the cations and anions results in the formation of a layered structure, comprised of alternating organic and inorganic layers, as illustrated in Fig. 6(a). Consecutive inorganic sheets are staggered as metal ions of adjacent inorganic layers do not align.

The inter-layer Mn–O···O–Mn contact distance is 8.327 Å and the layer repeat distance is 11.358 Å. The inorganic layer comprises hexa-coordinated metal ions. In each $[MnCl_4(H_2O)_2]^{2-}$ anion, two aqua ligands and four chlorido

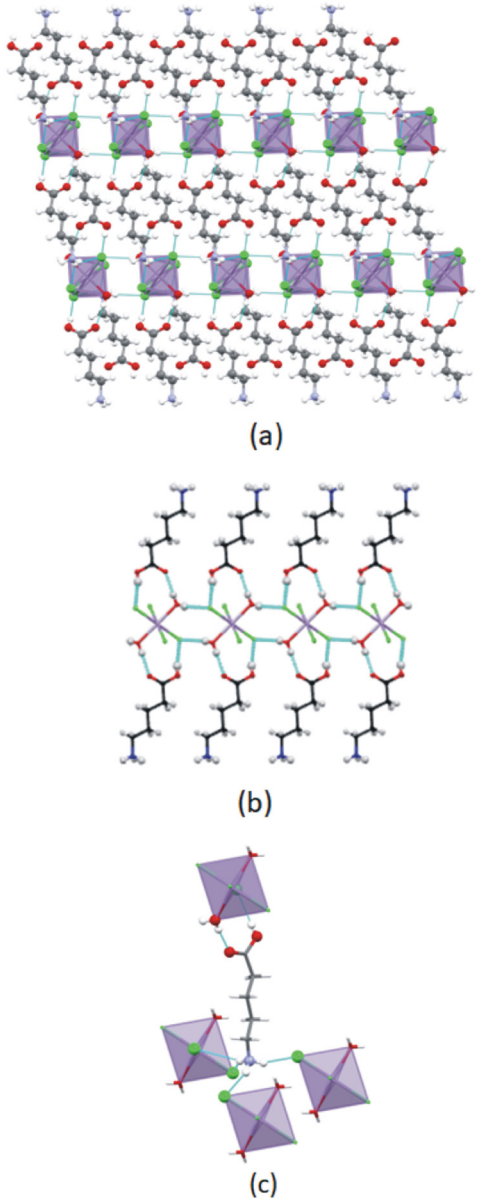

Fig. 6 (a) Packing diagram of, and hydrogen bonding network in structure **C5MnClH$_2$O**, viewed down the *b*-axis. Hydrogen bonding interactions are illustrated as blue dashed lines. (b) 1D hydrogen bonded ribbon formed along the *a*-direction in structure **C5MnClH$_2$O**. (c) Different types of hydrogen bonding interactions in structure **C5MnClH$_2$O**. The atoms involved in hydrogen bonding are indicated in ball representation while the rest of the atoms are shown in stick representation.

ligands are coordinated to the Mn^{2+} ion, *trans* to each other, resulting in an octahedral geometry.

Different types of hydrogen bonding interactions are present in the structure to form a 3D hydrogen bonded network, as shown in Fig. 6(a) to (c). These include N–$H^+\cdots^-$Cl–Mn, C–O–H$\cdots^-$Cl–Mn, Mn–O–H$\cdots^-$Cl–Mn and Mn–O–H$\cdots$O=C hydrogen bonding interactions. Unlike what was observed for structure **C3MnClH$_2$O**, no N–$H^+\cdots$O–Mn hydrogen bonds are present, making the hydrogen bonding network in structure **C5MnClH$_2$O** different from that formed in structure **C3MnClH$_2$O**.

The $[MnCl_4(H_2O)_2]^{2-}$ anions in the inorganic layer are cross-linked through Mn–O–H$\cdots^-$Cl–Mn hydrogen bonding interactions to form a 1D hydrogen bonded ribbon, as shown in Fig. 6(b). The ammonium group and carboxylic group of each cation is hydrogen bonded to consecutive inorganic layers, with the chlorido and aqua ligands of the anions accepting the hydrogen bonds, while the ammonium and carboxylic acid groups are hydrogen bonding donors.

The carboxylic acid group forms one C–O–H$\cdots^-$Cl–Mn interaction to an anion and accepts a C=O$\cdots$H–O–Mn hydrogen bond from the same anion, while the ammonium group forms two classical and one bifurcated, charge-assisted N–$H^+\cdots^-$Cl–Mn hydrogen bonding interactions to three different anions in two anionic hydrogen bonded ribbons, meaning that the ammonium groups straddle neighbouring anionic hydrogen bonded ribbons, to form a 3D hydrogen bonded network.

C4MnCl. **C4MnCl** crystallises in the monoclinic space group $P2_1/c$ and forms a 2D hybrid halide perovskite structure.[19] As shown in Fig. 1, the asymmetric unit comprises one 3-carboxypropylammonium cation and a $[MnCl_2]^-$ moiety, with the metal ion located on an inversion centre. Repetition of the inorganic portion of the asymmetric unit results in a 2D inorganic layer consisting of corner sharing, octahedral $[MnCl_6]^{4-}$ units. This inorganic layer is separated by a bilayer of cations, resulting in a layered, 2D hybrid halide perovskite structure, as shown in Fig. 7(a).

The 3-carboxypropylammonium cation deviates from the all-*trans* conformation, with a *gauche* orientation present in the cation, displaying a C1–C2–C3–C4 torsion angle of −73.25(18)°, as shown in Fig. 7(b).

The Mn–Cl$^-\cdots^-$Cl–Mn contact distance between consecutive inorganic layers is 11.005 Å, with a layer repeat distance of 15.945 Å. Consecutive inorganic layers are offset by (0.36,0.36), resulting in this structure being classified as a near-RP (nRP)[52] perovskite, since the offset is close to the offset of $(\frac{1}{3},\frac{1}{3})$ expected for an ideal RP structure. The staggered consecutive layers are illustrated in Fig. 7(c) and (d). The coordination sphere of the Mn^{2+} metal ion comprises six chlorido ligands forming the $[MnCl_6]^{4-}$ polyhedra. The Mn–Cl–Mn bridging angle is 167.097(13)°, and the ψ angle is 7.43°. The Mn^{2+} metal ions are uniformly separated along the *ab*-plane at 5.088 Å, and the metal ions, together with the bridging chlorido ligands create a 2D inorganic grid comprised of "squares" with approximate areas of 25.890 Å^2, calculated using the M$\cdots$M distances, as illustrated in Fig. 7(e). This 2D grid, together with the terminal halide ions, form a cavity into which the ammonium group penetrates slightly, as shown in Fig. 7(f), while it forms hydrogen bonding interactions to the terminal and/or bridging halides. The positive penetration depth of the ammonium group is 0.153 Å.

Two types of hydrogen bonding interactions are present in the structure. Firstly, the cations are connected to the

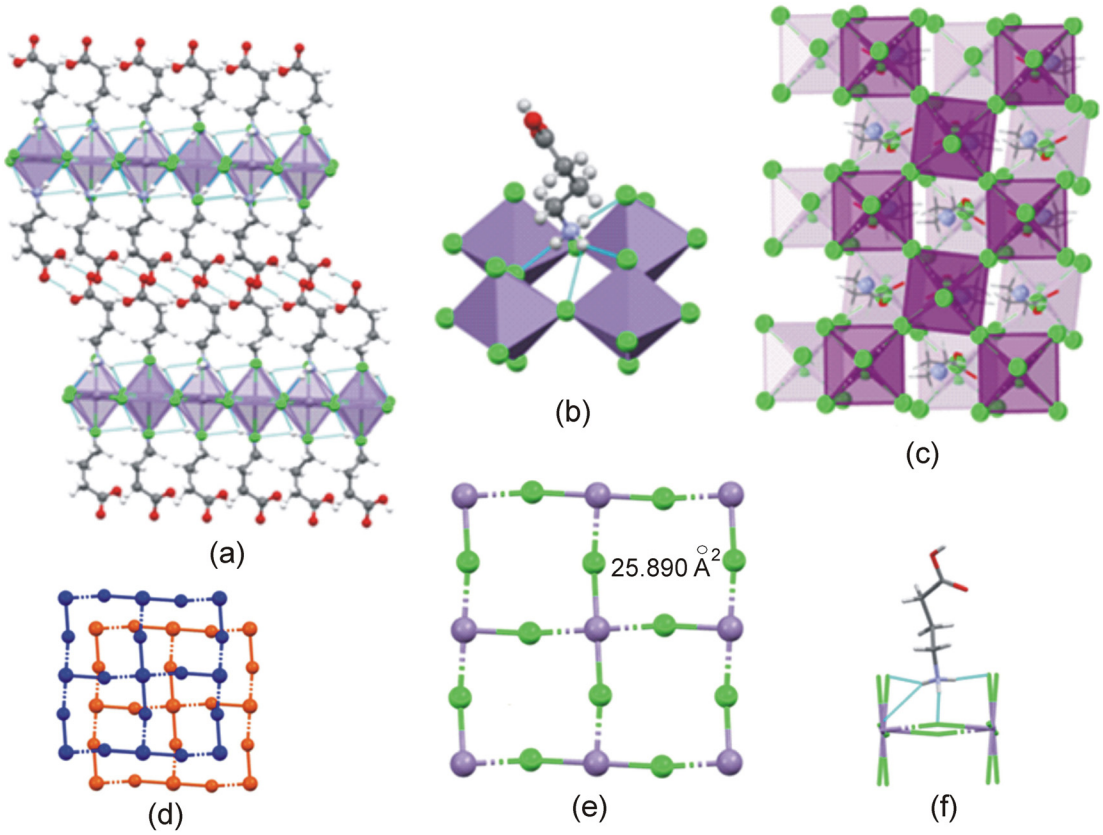

Fig. 7 (a) Packing diagram of structure **C4MnCl**, viewed down the *b*-axis, parallel to the inorganic layers. (b) *Gauche* bond in cation, and hydrogen bonding interactions in structure **C4MnCl**. Hydrogen bonds are indicated by blue dashed lines. (c) View of structure **C4MnCl** perpendicular to the inorganic layer, showing two consecutive, staggered inorganic layers, and the tilting of the polyhedra relative to each other. (d) Staggered arrangement of two consecutive inorganic layers, viewed perpendicular to the inorganic layer. Terminal halide ions are excluded for clarity. The top layer is shown in blue, and the bottom layer in orange. (e) 2D inorganic grid created by metal ions and bridging halide ligands. (f) Penetration of ammonium group into cavity created by metal ions and bridging and terminal halido ligands.

inorganic layer *via* charge-assisted N–H$^+\cdots^-$Cl–Mn hydrogen bonding interactions, with each ammonium group forming two classical and one bifurcated hydrogen bonds to two terminal and two bridging chlorido acceptors, as shown in Fig. 7(b), resulting in a 2D hydrogen bonding network. The β angle is 78.71°, the ϕ angle is 84.78°, and the hydrogen bonding configuration is t^2b. In addition, hydrogen bonded carboxylic acid dimers of the type O–H$\cdots$O=C are formed between carboxylic acid groups of adjacent cations in the organic layer, to form supramolecular cations of length 12.189 Å.

C6MnCl. The **C6MnCl** structure crystallises in the triclinic space group $P\bar{1}$, and forms a 2D hybrid halide perovskite structure.[19] The asymmetric unit comprises two crystallographically independent 5-carboxypentylammonium cations and one $[Mn_2Cl_4]^{2-}$ unit, as shown in Fig. 1. The crystallographically independent metal ions will be labelled Mn1 and Mn2. Both metal ions lie on inversion centres, and thus contribute only half their charge to the asymmetric unit, hence the charge of 2– for the $[Mn_2Cl_4]^{2-}$ unit. The two crystallographically independent cations will be distinguished based on their nitrogen atoms, with cation 1 containing atom N1, and cation 2 atom N2. Both cation 1 and cation 2 deviate from the all-*trans* conformation and display *gauche* bonds, however, the *gauche* bonds are in different positions in the two cations. In cation 1, the C2–C3–C4–C5 torsion angle deviates from 180°, with a value of −66.27(7)°, while in cation 2, the C7–C8–C9–C10 torsion angle has a value of 70.41(7)°.

Repetition of the inorganic part of the asymmetric unit results in the formation of an inorganic sheet consisting of corner sharing $[MnCl_6]^{4-}$ octahedra. The Mn$\cdots$Mn distances between metal ions bridged by halido ligands in the 2D inorganic layer are 5.152 Å and 5.033 Å in the *ab*-plane. The bridging Mn–Cl–Mn angles are 165.590(2)° (Mn1–Cl2–Mn3) and 164.430(2)° (Mn1–Cl2–Mn2), indicating the tilting of the octahedra relative to each other. The ψ angles are 7.63° for the octahedron containing ion Mn1 and 7.59° for the octahedron containing ion Mn2, resulting in corrugation of the inorganic layer.

The **C6MnCl** structure is layered, as illustrated in Fig. 8(a). The Mn–Cl$^-\cdots^-$Cl–Mn contact distance between neighbouring inorganic layers is 14.636 Å and the layer repeat distance is 19.624 Å.

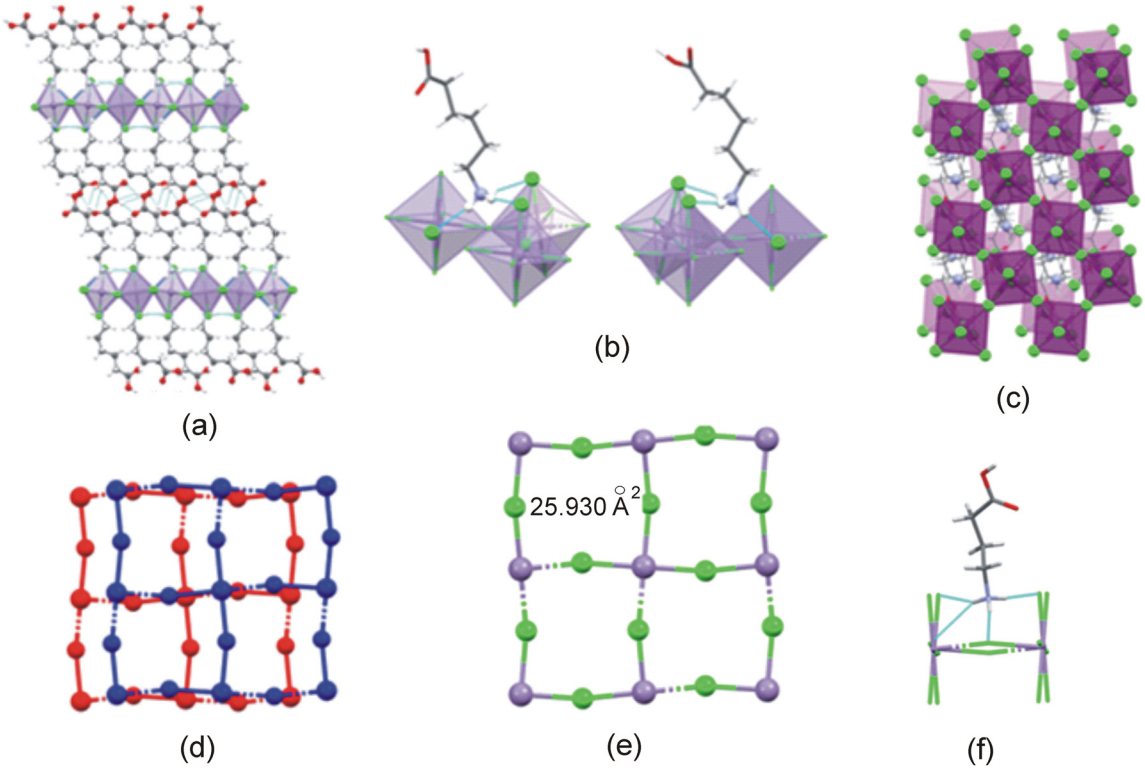

Fig. 8 (a) Packing diagram of structure **C6MnCl**, viewed down the *a*-axis, parallel to the inorganic layers. (b) Hydrogen bonding interactions involving (b) cation 1 and (c) cation 2 in the **C6MnCl** structure, indicated by blue dashed lines. The atoms involved in hydrogen bonding are indicated in ball representation while the rest of the atoms are shown in stick representation. (c) View of inorganic layers in structure **C6MnCl** perpendicular to the inorganic layers, showing two consecutive, staggered inorganic layers. (d) Staggered arrangement of two consecutive inorganic layers, viewed perpendicular to the inorganic layer. Terminal halide ions are excluded for clarity. The top layer is shown in blue, and the bottom layer in red. (e) 2D inorganic grid created by metal ions and bridging halido ligands. (f) Penetration of ammonium group into the cavity created by metal ions and bridging and terminal halido ligands. Hydrogen bonds are shown by blue dashed lines.

The ammonium groups from cations 1 and 2 anchor to the inorganic layer through strong, charge-assisted hydrogen bonding interactions of the type N–H$^+\cdots^-$Cl–Mn. Both cations from three classical hydrogen bonds to one bridging and two terminal chlorido ligands, as shown in Fig. 8(b). The hydrogen bonding configuration adopted is t^2b for both cations. The β angles are 69.28° and 69.56° for cation 1 and 2 and the ϕ angles are 68.02° and 68.42° for cation 1 and 2.

Adjacent cations in the organic layer are hydrogen bonded through O–H$\cdots$O=C hydrogen bonding interactions between carboxylic acid groups, to form supramolecular cations. The supramolecular cation chain lengths are 17.449 Å (cation 1 to cation 1) and 17.300 Å (cation 2 to cation 2).

Neighbouring inorganic layers are staggered, as illustrated in Fig. 8(c) and (d), with consecutive layers offset by (0.32,0.03). As such, the structure can be classified as a near-DJ (nDJ) perovskite,[52] since this offset is close to the offset of ($\frac{1}{2}$, 0) found for the ideal DJ perovskite.

The metal ions, together with the bridging chlorido ligands, create a 2D inorganic grid comprised of "squares" with areas of 25.930 Å^2, as illustrated in Fig. 8(e). The ammonium groups penetrate into the inorganic cavity, as shown in Fig. 8(f), forming hydrogen bonding interactions to the terminal and/or bridging halides. The positive penetration depths of the ammonium groups into the cavities are 0.168 Å and 0.166 Å for cations 1 and 2, respectively.

Structural comparison and discussion

In this section, the new structures determined in this study will be compared, structural trends identified, and comparisons made to structures reported in the literature, where applicable.

0D hybrid structures. **C3MnClH$_2$O** and **C5MnClH$_2$O** display similar 0D layered, hybrid structures, comprised of

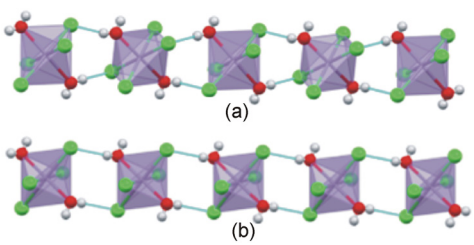

Fig. 9 Hydrogen bonded ribbon in structure (a) **C3MnClH$_2$O** and (b) **C5MnClH$_2$O**.

interdigitated all-*trans* *n*-carboxyalkylammonium cations and individual $[MnCl_4(H_2O)_2]^{2-}$ anions, as illustrated in Fig. 5(a) and 6(a).

The tilt angles of the polyhedra are similar in the **C3MnClH$_2$O** and **C5MnClH$_2$O** structures, at approximately 46°. Both compounds show staggered inorganic layers and a 1D hydrogen bonded ribbon is formed between the $[MnCl_4(H_2O)_2]^{2-}$ anions. However, in structure **C3MnClH$_2$O**, neighbouring anions in the ribbon alternate with respect to the orientation of their chlorido ligands, while they show the same orientation in structure **C5MnClH$_2$O**, as shown in Fig. 9(a) and (b). In both structures the carboxylic acid group forms a hydrogen bond to a chlorido ligand of an anion and accepts a hydrogen bond from a coordinated water molecule on the same anions, as illustrated in Fig. 5(c) and 6(c). However, they differ in terms of the hydrogen bonding interactions involving the ammonium group. In structure **C3MnClH$_2$O**, each ammonium group forms one hydrogen bond to a coordinated water molecule, and two hydrogen bonds to two different chlorido ligands, as shown in Fig. 5(c). In structure **C5MnClH$_2$O** each ammonium group forms three hydrogen bonds, one of which is bifurcated, to four different chlorido ligands, shown in Fig. 6(c). Hence, the overall hydrogen bonding networks formed in the two structures are different.

The ammonium group of each cation is hydrogen bonded to one inorganic layer, while its carboxylic acid group is hydrogen bonded to a neighbouring inorganic layer, and cation adopts an all-*trans* conformation in both structures.

A search of the CSD (Version 5.43, June 2022 update)[39] showed that only two structures containing only one type of organic cation and a $[MnCl_4(H_2O)_2]^{2-}$ anion have been reported in the literature. These structures are **EHIWIC**,[54] which contains an adamantanylammonium cation and **TAKZOV**,[55] that contains a carbamolguanidinium cation. In both literature structures the $[MnCl_4(H_2O)_2]^{2-}$ anion adopts a *trans* conformation, and the same 1D hydrogen bonded ribbon that is observed in structures **C3MnClH$_2$O** and **C5MnClH$_2$O**, is formed between the anions. As such, the formation of the $[MnCl_4(H_2O)_2]^{2-}$ anion is not very common.

2D hybrid halide perovskite structures. **C4MnCl** and **C6MnCl** both adopt a layered, 2D hybrid halide perovskite structure,[19] with inorganic layers comprised of corner sharing $[MnCl_6]^{4-}$ octahedra, separated by bilayers of non-interdigitated organic cations. In the organic layer of the two structures, the 3-carboxypropylammonium or 5-carboxypentylammonium cations adopt a *gauche* conformation, as illustrated in Fig. 10. The *gauche* conformation of the cation in structure **C4MnCl** and cation 2 in structure **C6MnCl** is at the same position relative to the ammonium group, while cation 1 in structure **C6MnCl** has a *gauche* conformation one bond further away from the ammonium group.

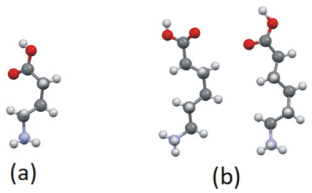

Fig. 10 Cation conformation in structure (a) **C4MnCl** and (b) **C6MnCl** (cation 1 left, cation 2 right).

The positioning of the ammonium ends of the cations is determined by the size of the square grid created by the metal ions and halide ions in the inorganic layer, with cations anchoring to neighbouring cavities created by these ions. *Gauche* bonds are introduced in the alkyl portions of the cations to increase their average thickness or diameter when the area of the square grid is larger than the average diameter of the all-*trans* cation, allowing the cation pack more efficiently in the organic layer. The average diameter of an all-*trans* alkyl chain is approximately 18–20 Å^2.[56] In structures **C4MnCl** and **C6MnCl** the areas of the square grids created in the inorganic layer are 25.890 Å^2 and 25.930 Å^2 respectively, which are larger than the average diameter of an all-*trans* alkyl chain, hence this leads to the introduction of *gauche* bonds in the cation to allow for better close packing of the alkyl portion of the *n*-carboxyalkylammonium cations in the organic layer.

The Mn–Cl–Mn bridging angle of structure **C4MnCl** (167.097(13)°) is slightly larger than those of structure **C6MnCl** (164.430(2)° and 165.590(2)°), indicating that the polyhedra are more tilted relative to each other in structure **C6MnCl**. The penetration depth of the cation in structure **C4MnCl** (0.153 Å) is slightly smaller than that of the cations in structure **C6MnCl** (0.166 Å and 0.168 Å), which agrees with reports in the literature that an increase in penetration depth of the cation is correlated with a smaller M–X–M angle.[52] The cations in the **C6MnCl** structure (β angles of 69.28° and 69.56°) are more tilted relative to the inorganic layer than the cations in the **C4MnCl** structure (β angle of 78.71°). Tilting of the cations also improves the close packing of the alkyl chains in the organic bilayer.

In both structures, the classic N–H$^+\cdots^-$Cl–Mn hydrogen bonding interactions adopt the t^2b configuration, and a carboxylic acid dimer hydrogen bond is present in the organic layer. The carboxylic acid dimer hydrogen bond links two *n*-carboxyalkylammonium cations into what can be viewed as a supramolecular cation. The supramolecular cation in the **C4MnCl** structure stretches athwart by one $[MnCl_6]^{4-}$ octahedron in the neighbouring inorganic layer, and the supramolecular cation in the **C6MnCl** structure by two octahedra.

The **C4MnCl** structure exhibits an offset of (0.36,0.36) of the Mn$\cdots$Mn distance between consecutive inorganic layers, making it a nRP perovskite, while structure **C6MnCl** displays an offset of (0.32,0.03), hence it can be classified as a nDJ perovskite structure.

A search of the Cambridge Structural Database (CSD) (Version 5.43, June 2022 update)[39] was conducted to find structures for *n*-alkylammonium or *n*-alkyldiammonium-

containing hybrid chloride 2D Mn^{2+} perovskites reported in the literature, with the search focussing in particular on structures containing either *n*-alkylammonium or *n*-alkyldiammonium cation and a Mn–Cl unit. Manual sifting of the structures was done to find only those structures exhibiting a 2D hybrid halide perovskite structure, with the formulae either $(NH_3(CH_2)_nCH_3)_2[MnCl_4]$ or $(NH_3(CH_2)_nNH_3)[MnCl_4]$. Only those with atomic coordinates reported were considered. The search revealed that the following compounds exhibit 2D hybrid halide perovskite structures, with the CSD[39] reference codes (refcodes) and the organic cation indicated: methylammonium: **MATCMN01**,[57] **MATCMN04**,[58] **MATCMN05**,[59] **MATCMN07**,[60] **MATCMN12**;[61] *n*-ethylammonium: **EAMNCL**,[62] and **EAMNCL11**,[63] *n*-propylammonium: **PAMMNC01**,[64] **PAMMNC10**,[65] **PAMMNC13**,[8] **PAMMNC36**;[66] *n*-decylammonium: **DECACM**,[67] **DECACM01**,[11] **DECACM02**,[11] and *n*-undecylammonium: **TAZQUJ**.[15]

n-Alkyldiammonium cation containing structures include: 1,2-ethyldiammonium: **ENDAMN10**[68] and **ENDAMN11**;[69] 1,3-propyldiammonium: **PYDAMN**,[70] and **PYDAMN03**;[71] 1,4-butyldiammonium: **BUCLMN**[72] and **BUCLMN01**;[72] 1,5-pentyldiammonum: **LUHCUO**,[73] **LUHCUO01**[74] and **LUHCUO02**[75] and 1,6-hexyldiammonium: **POCJOJ**.[76]

In addition to the *n*-alkylammonium or *n*-dialkylammonium-containing hybrid halide perovskite structures of Mn^{2+}, two other structure types with a Mn–Cl-containing anion and *n*-alkylammonium cation have been reported. One structure containing methylammonium cations combined with a 1D halide-bridged polymeric chain of the form $(Mn(H_2O)_2Cl_3)_\infty$ has been reported (**ZZZAXM01**,[77] **ZZZAXM02**[78]). In the polymer, chlorido ligands share corners, and pairs of ligands of the same type (chlorido or aqua) alternate along opposite sides of the chain. In addition, a structure comprised of *n*-decylammonium cations and isolated, tetrahedral $[MnCl_4]^{2-}$ anions has been reported (**TAZQOD**).[15]

However, for all the structures containing *n*-alkyldiammonium cations and a perchloridomanganate anion, only the 2D hybrid halide perovskite structure has been reported. In summary, the CSD search revealed that the 2D hybrid halide perovskite structure is by far the preferred structure formed on combination of *n*-alkylammonium or *n*-alkyldiammonium cations and perchloridomanganate anions.

Table 3 Classification of *n*-alkylammonium and *n*-alkyldiammonium-containing perchloridomanganate perovskite structures reported in the literature, and structures determined in this study

CSD Refcode	Cation	Space group and temperature	Offset	Staggered/eclipsed	Classification	Ref.
n-Alkyldiammonium cations						
ENDAMN10	1,2-Ethyldiammonium	$P2_1/b$ (295 K)	(0,0)	Eclipsed	Ideal DJ	68
ENDAMN11		$P2_1/c$ (100 K)				79
PYDAMN	1,3-Propyldiammonium	*Imma* (295 K)	(0,0)	Eclipsed	Ideal DJ	70
PYDAMN03		*Pnma* (295 K)				71
BUCLMN	1,4-Butyldiammonium	$P2_1/b$ (295 K)	(0,0)	Eclipsed	Ideal DJ	72
BUCLMN01		*Pnmb* (404 K)				72
LUHCUO	1,5-Pentyldiammonium	$I2_12_12_1$ (298 K)	(0,0)	Eclipsed	Ideal DJ	73
LUHCUO01		*Imma* (333 K)				74
LUHCUO02		*Pnma* (173 K)				75
POCJOJ	1,6-Hexyldiammonium	$P2_1/c$ (295 K)	(0,0)	Eclipsed	Ideal DJ	76
n-Alkylammonium cations						
MATCMN01	Methylammonium	*Abma* (295 K)	$(\frac{1}{2},\frac{1}{2})$	Staggered	Ideal RP	57
MATCMN04		*Pccn* (188 K)				58
MATCMN05		$I4/m$ (404 K)				59
MATCMN07		$P4_2/ncm$ (188 K)				60
MATCMN12		*Bmab* (295 K)				61
EAMNCL	*n*-Ethylammonium	*Abma* (295 K)	$(\frac{1}{2},\frac{1}{2})$	Staggered	Ideal RP	62
EAMNCL11		*Pbca* (126 K)[63]				63
PAMMNC01	*n*-Propylammonium	*Abma* (182 K)	(0,0)	Eclipsed	Ideal DJ	64
PAMMNC10	*n*-Propylammonium	*Cmca* (295 K)	$(\frac{1}{2},\frac{1}{2})$	Staggered	Ideal RP	65
PAMMNC13		$P2_1/b$ (8 K)				8
PAMMNC36		*Abma* (365 K)				66
DECACM	*n*-Decylammonium	$P2_1/a$ (283 K)	(0.35,0.35)	Staggered	Ideal RP	67
DECACM01		$P2_1/a$ (283 K)	(0.35,0.35)			11
DECACM02		$C2/m$ (330 K)	$(\frac{1}{2},\frac{1}{2})$			11
TAZQUJ	*n*-Undecylammonium	$P2_1/c$ (293 K)	(0.26,0.42)	Staggered	nRP	15
n-Carboxyalkylammonium cations						
C4MnCl	3-Carboxylpropylammonium	$P2_1/c$ (150 K)	(0.36,0.36)	Staggered	nRP	This study
C6MnCl	5-Carboxylpentylammonium	$P\bar{1}$ (150 K)	(0.32,0.03)	Staggered	nDJ	This study

For comparison purposes, the offset in structures of 2D hybrid perchloridomanganate perovskites containing *n*-alkylammonium or *n*-alkyldiammonium cations reported in the literature were determined, and they were classified as DJ, RP, nDJ or nRP perovskites.[52] The results of the analysis are tabulated in Table 3.

As can be seen from the results in Table 3, all the *n*-alkyldiammonium-containing perchloridomanganate hybrid halide perovskite structures display a (0,0) offset of their inorganic layers, hence the ideal DJ structure is adopted, as expected for dication-containing perovskites.

Most *n*-alkylammonium-containing perchloridomanganate hybrid halide perovskite structures display a $(\frac{1}{2},\frac{1}{2})$ offset of the inorganic layers, thus forming the ideal RP structure, as expected for monocation-containing perovskites, however, there are some exceptions.

Firstly, two types of structures have been reported for the *n*-decylammonium containing analogue. These structures were determined at different temperatures and represent thermotropic polymorphs. One of the structures, **DECACM02**,[68] determined at 330 K, displays the expected RP structure with an $(\frac{1}{2},\frac{1}{2})$ offset. The second structure (**DECACM**[67] and **DECACM01**[68]), determined at 283 K, exhibits an offset of (0.35,0.35), which indicates a nRP perovskite. The structure **TAZQUJ**,[15] containing *n*-undecylammonium cations, displays an offset of (0.26,0.26), hence it is a nRP perovskite. It is noteworthy that both structures that display nRP perovskite structures contain long-chain *n*-alkylammonium cations. A third exception is structure **PAMMNC01**,[64] determined at 182 K, which contains an *n*-propylammonium cation, and displays a (0,0) offset, making it an ideal DJ perovskite, despite the presence of a monocation in the structure. However, three ideal RP structures have also been reported for this compound, determined at three different temperatures, spanning a wide temperature range, namely **PAMMNC10**[65] (determined at 295 K), **PAMMNC1**[38] (determined at 8 K) and **PAMMNC36**[66] (determined at 365 K). It is unclear why the compound exhibited an ideal RP structure over such a wide temperature range, but an ideal DJ structure at 182 K.

In summary, all the *n*-alkyldiammonium-containing perchloridomanganate structures considered form ideal DJ structures, and most of the *n*-alkylammonium-containing structures form ideal RP structures, as expected. Two of the exceptions can be ascribed to the presence of long-chain *n*-alkylammonium cations, and increased flexibility in the longer cationic chains. Thus, as the length of the *n*-alkylammonium chain increases, a nRP instead of an ideal RP structure is formed.

Structure **C4MnCl** also forms a nRP perovskite structure, while structure **C6MnCl** exhibits a nDJ perovskite structure. Both structures contain *n*-carboxyalkylammonium monocations, and based on this, a RP structure is expected. However, since a supramolecular cation is formed in these structures *via* hydrogen bonded carboxylic acid groups, the supramolecular cation may be viewed as a diammonium dication, in which case a DJ structure is expected.

However, neither the ideal DJ or ideal RP perovskite structure is formed for **C4MnCl** or **C6MnCl**. This means that the change of one terminal functional group from an ammonium group in an *n*-alkyldiammonium cation, or a methyl group in an *n*-alkylammonium cation, to a carboxylic acid group, impacts on the relative orientation of the inorganic layers in the structures **C4MnCl** and **C6MnCl**, and a results in a deviation from the ideal RP or ideal DJ structures to form either a nRP or nDJ structure, and may be used as a structure manipulation tool.

Structural types

0D and 2D structures. An interesting observation from this study is the fact that two different types of structures are formed from the self-assembly of *n*-carboxyalkylammonium cations and $MnCl_2$-based anions, even though the compounds were prepared using the same ratio of reagents and experimental methodology.

A prominent odd–even effect is displayed in the structures under investigation. When the number of carbon atoms in the *n*-carboxyalkylammonium cation is odd, *i.e.*, structures **C3MnClH$_2$O** and **C5MnClH$_2$O**, a 0D organic–inorganic hybrid structure is formed, with water molecules forming part of the coordination sphere of the Mn^{2+} ion, resulting in isolated $[MnCl_4(H_2O)_2]^{2-}$ anions. Even though water was not used specifically as a reagent in the reaction, water molecules were present as part of the concentrated HCl used in the reaction. However, when an even number of carbon atoms are present in the *n*-carboxyalkylammonium cation, *i.e.*, structures **C4MnCl** and **C6MnCl**, the hybrid halide perovskite structure is formed, and no water molecules are incorporated into the structure, even though water molecules were available as part of the concentrated acid.

Both structure types are layered but differ in terms of the type of inorganic anion formed, the packing of ions and hydrogen bonding interactions. A 2D inorganic layer consisting of corner-sharing $[MnCl_6]^{4-}$ octahedra is formed in the 2D hybrid halide perovskite structures, **C4MnCl** and **C6MnCl**, while the inorganic layer comprises isolated 0D $[MnCl_4(H_2O)]^{2-}$ anions in the odd-chain containing compounds **C3MnClH$_2$O** and **C5MnClH$_2$O**.

In the 2D hybrid halide perovskite-type structures, a bilayer of non-interdigitated organic cations is formed, with the ammonium groups hydrogen bonding to the inorganic layer, and the carboxylic acid groups forming a separate hydrogen bonded layer comprised of hydrogen bonded carboxylic acid dimers as part of the organic layer. However, in the 0D structures, the cations are interdigitated, and all the functional groups capable of hydrogen bonding (*i.e.*, the carboxylic acid group, ammonium group and anion), form a single hydrogen bonded network.

In order to understand the preference for a certain structural type based on the number of carbon atoms in the

Table 4 Results of a CSD (Version 5.43, June 2022 update)[39] search of 2D hybrid halide perovskite structures containing 2-carboxyethylammonium or 4-carboxybutylammonium cations

CSD Refcode	Cation	Metal ion	Halido ligand	Ref.
BEHXIV **BEHXIV01**	2-Carboxyethylammonium	Cu^{2+}	Cl^-	80 and 81
CAYPOH	2-Carboxyethylammonium	Cu^{2+}	Br^-	82
KETHID	4-Carboxybutylammonium	Pd^{2+}	Cl^-	83
VUHVIG **VUHVIG01** **VUHVIG02**	4-Carboxybutylammonium	Pb^{2+}	Cl^-	84–86
VUHVUS **VUHVUS01** **VUHVUS02**	4-Carboxybutylammonium	Pb^{2+}	Br^-	84, 85 and 87

n-carboxyalkylammonium chain, it is informative to consider some related structures reported in the literature.

As noted previously, a search of the CSD[39] indicated that compounds of this type containing *n*-alkyldiammonium chains all form the 2D hybrid halide perovskite structure. For compounds containing *n*-alkylammonium chains, the 2D hybrid perovskite structure is by far the preferred structure type, with only two exceptions reported in the literature, namely one with a tetrahedral $[MnCl_4]^{2-}$ anion (**TAZQOD**[15]) and one with a 1D polymeric $[Mn(H_2O)_2Cl_3]_\infty$ anion (**ZZZAXM01** (ref. 77) and **ZZZAXM02** (ref. 78).

The question can be asked if it is possible to form a 2D hybrid halide perovskite structure containing the odd numbered cations 2-carboxyethylammonium or 4-carboxybutylammonium. A search of the CSD (Version 5.43, June 2022 update)[39] reveals that 2D hybrid halide perovskite structures containing these cations have indeed been reported in the literature for a range of metal ions and halido ligands, as listed in Table 4.

Thus, it is possible to incorporate these cations containing an odd number of carbon atoms into the perovskite structure, however, this does not occur when the metal ion is Mn^{2+} and the halido ligand is a chlorido ligand. Rather than a 2D perovskite structure forming, where only halide ions are coordinated to the Mn^{2+} ion, isolated $[MnCl_4(H_2O)_2]^{2-}$ anions are formed *via* the coordination of water molecules to the Mn^{2+} ion. This process can be seen as dimensional reduction from the 2D hybrid perovskite structure, which contains a $[MnCl_4]^{2-}$ repeat unit, to form a $[MnCl_4(H_2O)_2]^{2-}$ anion, through replacement of two corner sharing chlorido ligands with terminal aqua ligands and changing two other corner sharing chlorido ligands to terminal chlorido ligands.

Anions of the formula $[MCl_4(H_2O)_2]^{2-}$, in either the *cis*- or *trans* conformation, where M is any metal ion, are relatively rare. A search of the CSD (Version 5.43, June 2022 update)[39] was conducted to find any structures containing either *cis*- or *trans* anions of this type containing any metal ion, in combination with any other species, with the results of the search listed in ESI† Section S3. The results from the search revealed that only 32 structures containing this type of anion have been reported. *Trans*-$[MCl_4(H_2O)_2]^{2-}$ anions have been reported for the following metal cations, with the number of structures reported in the CSD[39] indicated in parenthesis: Mn^{2+} (5), Sn^{4+} (2), Fe^{3+} (2), Ca^{2+} (1), Cu^{2+} (1), Fe^{2+} (1), In^{3+} (1), Co^{2+} (1), Rh^{3+} (1), Cd^{2+} (1). The *cis* analogues of the $[MCl_4(H_2O)_2]^{2-}$ anions have been reported for the following metal ions, with the number of structures containing this anion indicated in parenthesis: Sn^{4+} (8), In^{3+} (3), Rh^{3+} (1), Pt^{4+} (1), Tc^{4+} (1), Mn^{2+} (1), Ru^{3+} (1). Thus, the formation of this type of anion is quite rare. The reason for the formation of this specific anion in the structures in which the cation contains an odd number of carbon atoms is unclear, and it can only be noted. The odd–even effect is well known for compounds containing *n*-alkyl portions, where compounds with an even number of carbon atoms display a different type of structure compared to those with an odd number of carbon atoms, with each family forming a homologous structural series.[36–39]

Thus, even though *n*-alkylammonium- and *n*-alkyldiammonium-containing perchloridomanganate compounds show a clear preference for the hybrid halide perovskite structure, this structure is only preferred for the *n*-carboxyalkylammonium containing perchloridomanganate compounds with an even number of carbon atoms in the chain.

Interdigitation of *n*-carboxyalkylammonium chains. A major difference between the 0D and 2D structures is the interdigitation of the *n*-carboxyalkylammonium cations in the 0D structures to form a single organic layer, and the non-interdigitation of these cations in the 2D hybrid halide perovskite structures to form an organic bilayer.

A study[33] considering salts of *n*-carboxylalkylammonium cations containing an even number of carbon atoms showed that, depending on the type of anion present, either an organic bilayer structure, similar to the organic layer in the 2D hybrid halide perovskite structures reported here, or an interdigitated organic layer, similar to the organic layer of the 0D structures reported here, may be formed. It was found the structures containing chloride and bromide anions showed interdigitated *n*-carboxyalkylammonium chains, and a single hydrogen bonding network, similar to the cation packing in structures **C3MnClH$_2$O** and **C5MnClH$_2$O**. However, the structures containing nitrate and perchlorate anions formed non-interdigitated, bilayer structures, with carboxylic acid dimers forming in the organic layer, similar to what is observed in structures **C4MnCl** and **C6MnCl**. Thus, the specific anion present in the structure plays a role in whether a structure with interdigitated *n*-carboxyalkylammonium chains, like the 0D structures reported here, or a non-interdigitated structure, similar to the 2D perovskite type structures reported here, is formed. This observation was attributed to the hydrogen bonds formed between the cations and anions in these structures, and the effect of anion size on the hydrogen bonding network.

In the current series the interdigitation or non-interdigitation of the cations can also be explained by

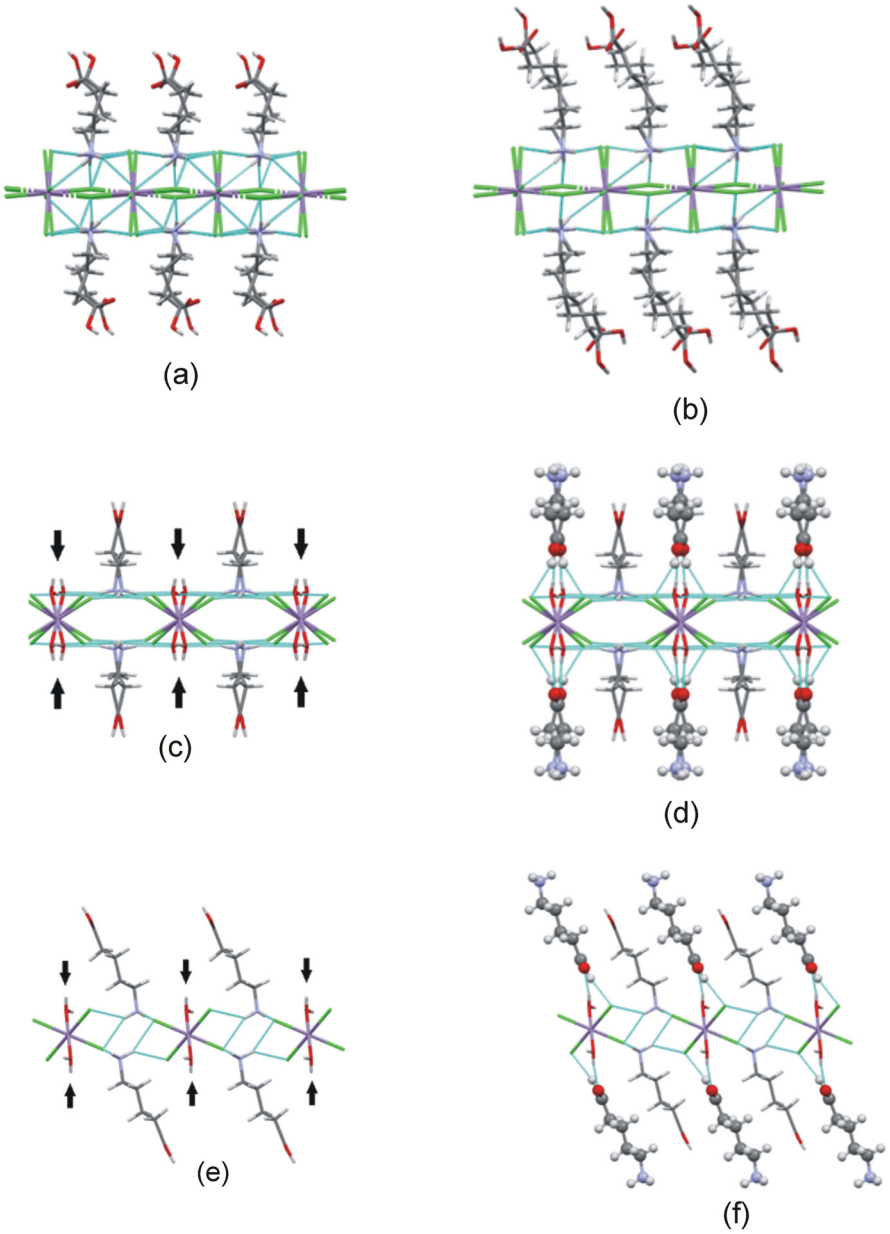

Fig. 11 Primary hydrogen bonding network in structure (a) **C4MnCl** and (b) **C6MnCl**. (c) Primary hydrogen bonding network in structure **C3MnClH$_2$O**. Arrows indicate available hydrogen bonding sites in the primary network. (d) Cations shown in ball-and-stick representation are hydrogen bonded to the sites indicated by arrows in figure (c). (e) Primary hydrogen bonding network in structure **C5MnClH$_2$O**. Arrows indicate available hydrogen bonding sites on the primary network. (f) Cations shown in ball-and-stick representation are hydrogen bonded to the sites indicated by arrows in figure (e).

considering the hydrogen bonding network formed in the two structural types. Etter[88] stated that the strongest hydrogen bond donor will hydrogen bond to the strongest hydrogen bond acceptor. In the structures under investigation, the strongest hydrogen bonding donor is the ammonium group, and the strongest hydrogen bonding acceptor is the coordinated chlorido ligands, due to the charge assisted nature of the N–H$^+\cdots^-$Cl–Mn hydrogen bonds that can form between these species.[89] The rule provided by Etter[88] can be applied to define a primary hydrogen bonding network in both the 0D and the 2D structure types, *i.e.* the hydrogen bonding network formed between the ammonium groups and the chlorido ligands represent the primary network. Other hydrogen bonding species that form weaker hydrogen bonds can then also form or accept hydrogen bonds to or from this primary network, provided there is space accessible on the primary network for additional hydrogen bonding interactions to occur. If no space is available, the weaker groups will form a separate hydrogen bonding network.

The primary hydrogen bonding network formed between ammonium groups and halido ligands in structure **C4MnCl**

is shown in Fig. 11(a), viewed down an arbitrary axis to show the ammonium groups anchoring to the cavities created in the inorganic layer. From this figure it is clear that all available hydrogen bonding acceptor sites on the inorganic layer are occupied by ammonium groups, hence no sites are available for carboxylic acid groups to form hydrogen bonds to the inorganic layer. As a result, the carboxylic acid groups cannot hydrogen bond to the primary hydrogen bonding layer, and instead form carboxylic acid dimers in the organic layer due to their donor and acceptor character,[33] with is the only option available to satisfy the hydrogen bonding capability of the carboxylic acid functional groups, and a non-interdigitated, organic bilayer is formed. The same argument holds for structure **C6MnCl**, with the primary network illustrated in Fig. 11(b), resulting in the formation of a non-interdigitated organic bilayer.

The primary hydrogen bonding network formed in structure **C3MnClH$_2$O** between the ammonium group donors and chlorido acceptors is illustrated in Fig. 11(c). As indicated by the arrows in Fig. 11(c), the sites above the coordinated water molecules in this network are unoccupied and are available to accept and donate hydrogen bonds to the carboxylic acid groups of cations of which the ammonium groups form part of a neighbouring primary network. Fig. 11(d) shows the cations hydrogen bonded to the primary network *via* their carboxylic acid groups. The same is true for structure **C5MnClH$_2$O**, as illustrated in Fig. 11(e) and (f). As a result, cations are hydrogen bonded to one primary network *via* their ammonium groups and to a neighbouring primary network *via* their carboxylic acid groups, resulting in interdigitated structures. Hence, the nature of the primary hydrogen bonding network and the type of inorganic layer formed play an important role in determining whether an interdigitated or non-interdigitated structure is formed.

In both structure types, the effect of the hydrogen bonds involving the carboxylic acid groups is to "zipper" neighbouring primary networks together, either through the formation of an interdigitated structure where the carboxylic acid groups hydrogen bond to the primary hydrogen bonding network, or through the formation of a non-interdigitated bilayer structure, where carboxylic acid dimers are formed in the organic layer.

Magnetic characterisation

All four compounds structurally characterised were also characterised magnetically by SQUID magnetometry.

C3MnClH$_2$O and C5MnClH$_2$O. The magnetic susceptibility of **C3MnClH$_2$O** and **C5MnClH$_2$O** were measured in the region 1.8 K to 310 K. The $\chi(T)$, $\chi T(T)$ and $\chi^{-1}(T)$ data of **C3MnClH$_2$O** and **C5MnClH$_2$O** are shown in Fig. 12(a) and (b). *M vs. H* plots are given and discussed in ESI† Section S4.

Paramagnetic behaviour is observed at higher temperatures, with a χT value of 4.26 cm^3 K mol^{-1} for **C3MnClH$_2$O** and 4.57 cm^3 K mol^{-1} for **C5MnClH$_2$O** at 310 K. These values are close to the expected value of 4.375 cm^3 K mol^{-1} for a Mn^{2+} ion of $S = 5/2$. Below 25 K for **C3MnClH$_2$O** and 36 K for **C5MnClH$_2$O**, the χT values show gradual decrease followed by a sharper decrease, which is indicative of AFM interactions between the Mn^{2+} ions or possibly single ion anisotropy (SIA) due to the polyhedra not being truly octahedral.

A Curie–Weiss analysis of the $\chi^{-1}(T)$ plots (Fig. 12(a) and (b)) was done for **C3MnClH$_2$O** between 77 K and 310 K, and for **C5MnClH$_2$O** between 122 K and 310 K.

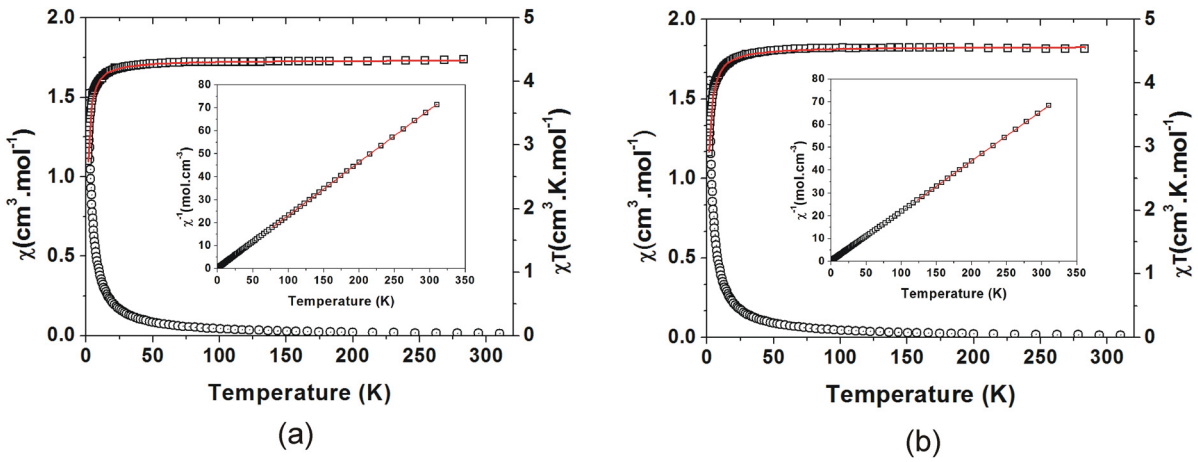

Fig. 12 (a) $\chi(T)$ (O) and $\chi T(T)$ (□) plots for **C3MnClH$_2$O** between 1.8 K and 310 K. The red line through the data points corresponds to the fit of the $S = 5/2$ AFM chain model. The insert shows the $\chi^{-1}(T)$ plot for **C3MnClH$_2$O** between 1.8 K and 310 K. The red line through the data points corresponds to a linear fit between 77 K and 310 K. (b) $\chi(T)$ (○) and $\chi T(T)$ (□) plots for **C5MnClH$_2$O** between 1.8 K and 310 K. The red line through the data points corresponds to the fit of the $S = 5/2$ AFM chain model. The insert shows the $\chi^{-1}(T)$ plot for **C5MnClH$_2$O** between 1.8 K and 310 K. The red line through the data points corresponds to a linear fit between 122 K and 310 K.

Table 5 Summary of magnetic parameters

Compound	**C3MnClH$_2$O**	**C5MnClH$_2$O**	**C4MnCl**	**C6MnCl**
$2J_K$ (K)	−0.14(2)	−0.14(2)	−8.28(5)	−7.72(4)
Exchange	AFM	AFM	AFM	AFM
g	—	—	1.96(8)	1.94(6)
Curie constant (mol cm^{-3})^a	4.33(1)	4.55(3)	—	—
Curie constant (mol cm^{-3})^b	4.34(2)	4.52(2)	5.16(2)	4.53(2)
θ (K)	−0.98(3)	−0.83(3)	−190(5)	−175(5)
Model	1D AFM chain[90]	1D AFM chain[90]	AFM square lattice[94]	AFM square lattice[94]
T_N (K)	—	—	45.0(5)	43(1)
$T(\chi_{max})$ calc (K)	—	—	83	89
$T(\chi_{max})$ exp (K)	—	—	83	87

^{a} Curie constant obtained from fitting to model. ^{b} Curie constant obtained from Curie–Weiss analysis.

Due to the plots not being perfectly linear, approximate Curie constants of 4.34(2) cm^3 K mol^{-1} and 4.52(2) cm^3 K mol^{-1} were obtained for **C3MnClH$_2$O** and **C5MnClH$_2$O**, with negative Weiss temperatures, θ, of −0.98(3) K and −0.83(3) K, indicating AFM behaviour.

Structures **C3MnClH$_2$O** and **C5MnClH$_2$O** contain 1D hydrogen bonded chains, with neighbouring Mn^{2+} ions linked *via* Mn–O–H$\cdots^{-}$Cl–Mn hydrogen bonds. The experimental susceptibility data was fitted to a model for a S = 5/2 AFM chain.[90] This model is based on the Hamiltonian $H = -\sum_{nn} 2J_K S_i S_j$ with $\sum_{nn}$ running over all possible pairs of nearest-neighbour spins i and j, with a negative J_K value indicating AFM interactions. The model is given by eqn (1):

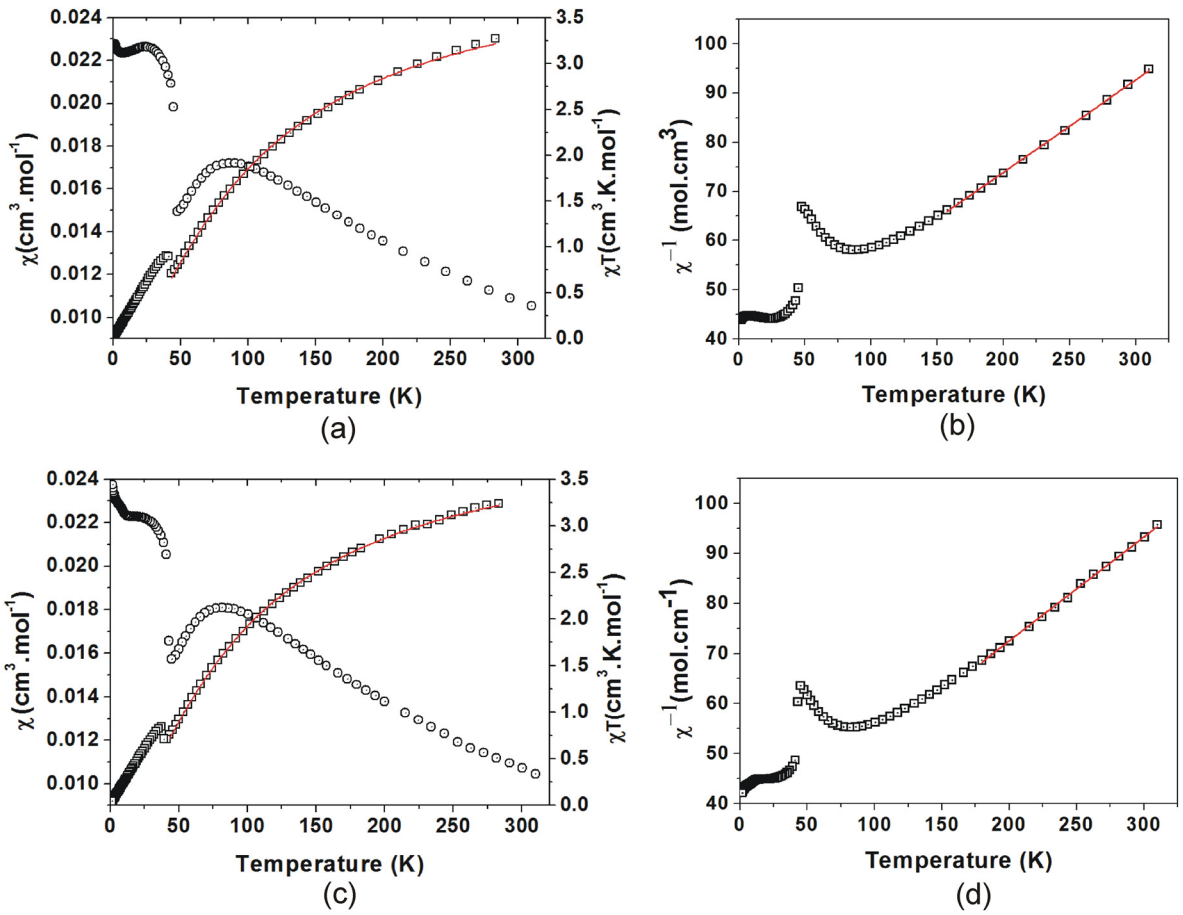

Fig. 13 (a) $\chi(T)$ (□) and $\chi T(T)$ (○) plots for **C4MnCl** between 1.8 K and 310 K. The red line through the data points corresponds to the fit of the S = 5/2 AFM square lattice model from T_N to 310 K. (b) $\chi^{-1}(T)$ plot for **C4MnCl** between 1.8 K and 310 K. The red line through the data points corresponds to a linear fit between 157 K and 310 K. (c) $\chi(T)$ (□) and $\chi T(T)$ (○) plots for **C6MnCl** between 1.8 K and 310 K. The red line through the data points corresponds to the fit of the S = 5/2 AFM square lattice model from T_N to 310 K. (d) $\chi^{-1}(T)$ plot for **C6MnCl** between 1.8 K and 310 K. The red line through the data points corresponds to a linear fit between 180 K and 310 K.

$$\chi T = \frac{NS(S+1)}{3k} g^2\beta^2 \frac{1+u(K)}{1-u(K)} \quad (1)$$

where $u(K) = \coth K - \frac{1}{K}$ and $K = -2J_K S(S+1)/kT$.

Here, N is Avogadro's constant, β the Bohr magneton, k the Boltzmann's constant, J_K the exchange parameter, $g = 2$ and $S = 5/2$. On substitution of the constants, eqn (2) is obtained:

$$\chi T = CC\left(\frac{1-\coth\left(\frac{17.5J_K}{T}\right)+\left(\frac{0.0571T}{J_K}\right)}{1+\coth\left(\frac{17.5J_K}{T}\right)-\left(\frac{0.0571T}{J_K}\right)}\right) \quad (2)$$

where CC is the Curie constant and J_K the magnetic exchange parameter. Both CC and J_K are allowed to vary, with CC constrained to fall between 3 and 5 K. The values obtained for the parameters are listed in Table 5.

The fits of the $\chi T(T)$ data of **C3MnClH$_2$O** and **C5MnClH$_2$O** to this model are shown in Fig. 12(a) and (b), and the values obtained through the fits are listed in Table 5. A value of $2J_K$ equal to −0.14(2) K and a Curie constant of 4.33(1) cm^3 K mol^{-1} were obtained for **C3MnClH$_2$O**, and $2J_K$ equal to −0.14(2) K and a Curie constant of 4.55(3) cm^3 K mol^{-1} was found for **C5MnClH$_2$O**, with the negative $2J_K$ values indicating AFM interactions or SIA interactions. The small values of the exchange parameters indicate weak magnetic exchange interactions *via* the Mn–O–H$\cdots$Cl–Mn hydrogen bonding interactions linking Mn^{2+} ions.

C4MnCl and C6MnCl. The temperature dependent magnetic susceptibility of **C4MnCl** and **C6MnCl** were measured in the region 1.8 K to 310 K. The $\chi(T)$, $\chi T(T)$ and $\chi^{-1}(T)$ plots of **C4MnCl** and **C6MnCl** are shown in Fig. 13(a) to (d). Both compounds show a broad maximum in their magnetic susceptibility as a function of temperature curves (Fig. 13(a) and (c)) which is indicative of AFM interactions in the inorganic layer.

The $\chi(T)$ plots (Fig. 13(a) and (c)) both show a gradual increase from 0.011 cm^3 mol^{-1} at 310 K, with a broad maximum of 0.017 cm^3 mol^{-1} at 87 K for **C4MnCl** and 0.018 cm^3 mol^{-1} at 83 K for **C6MnCl**. On further cooling, the susceptibility of both compounds shows a decrease followed by a sharp increase at the Neél temperature, T_N, and a steep rise below T_N, which signifies spontaneous magnetisation as a result of long range 3D AFM ordering due to spin canting,[91] with T_N = 45.0(5) K for **C4MnCl** and T_N = 43(1) K for **C6MnCl**, respectively. The spin canting is attributed to antisymmetric Dzyaloshinskii–Moriya interactions that occur due to the tilting of the $[MnCl_6]^{4-}$ octahedra in the inorganic plane.[26,92] Further cooling results in a continued increase in susceptibility.

The $\chi T(T)$ plots (Fig. 13(a) and (c)) show values of 3.35 cm^3 K mol^{-1} and 3.32 cm^3 K mol^{-1} for **C4MnCl** and **C6MnCl** respectively at 310 K, which is lower than the expected value of 4.375 cm^3 K mol^{-1} for Mn^{2+}. On cooling from 310 K, the $\chi(T)$ data show a gradual decrease to reach a minimum at T_N = 45.0(5) K for **C4MnCl** and T_N = 43(1) K for **C6MnCl**, where after there is a sharp increase. This is followed by a further decrease on cooling, approaching zero, for both compounds.

A Curie–Weiss analysis of the $\chi^{-1}(T)$ plots was done for **C4MnCl** between 157 K and 310 K, and for **C6MnCl** between 180 K and 310 K. At high temperatures there is no region where $\chi T(T)$ is constant, thereby completely obeying Curie–Weiss law. Thus, the Curie–Weiss values obtained serve merely as an approximation. From the Curie–Weiss plots (Fig. 13(b) and (d)), approximate Curie constants of 5.16(2) mol cm^{-3} and 4.53(2) mol cm^{-3} were obtained for **C4MnCl** and **C6MnCl**, with approximate Weiss temperatures, θ, of −190(5) K and −175(5) K, with the negative Weiss temperatures indicating AFM behaviour.

C4MnCl and **C6MnCl** adopt the 2D perovskite structure and since they contain Mn^{2+} ions, are expected to behave as 2D $S = 5/2$ Heisenberg antiferromagnets at low temperature. The intra-planar AFM exchange interactions occur through the single-halide, Mn–Cl–Mn superexchange pathway where bridging halido ligands link neighbouring Mn^{2+} ions to form a square lattice. The magnetic d orbitals of neighbouring metal ions overlap *via* the common orbital of the bridging halido ligand. Inter-layer magnetic coupling occurs at low temperature and is expected to be much smaller than intra-layer coupling, by at least a factor (10^4),[93] and is seen as negligible.

Since the **C4MnCl** and **C6MnCl** systems can be treated as AFM square lattices, the magnetic susceptibility data was fit to a model for a $S = 5/2$ square lattice of classical spins, based on the $2J_K$ Hamiltonian $H = -\sum_{nn} 2J_K S_i S_j$, with $\sum_{nn}$ running over all possible pairs of nearest-neighbours spins i and j, with a negative $2J_K$ value indicating an AFM interaction, given by eqn (3):[94]

$$\chi T = \frac{Ng^2\beta^2 S(S+1)(1+u)^2}{3k(1-u)^2} \quad (3)$$

with $u = \coth[(J_K S(S+1))/kT] - \frac{kT}{J_K S(S+1)}$ where, N is Avogadro's constant, g the g factor, β the Bohr magneton, k the Boltzmann's constant, J_K the magnetic exchange parameter and $S = 5/2$.

On substitution of the constants, eqn (4) is obtained:

$$\chi T = 1.1825g^2\left(\frac{\left(1+\coth\left(\frac{17.5J_K}{T}\right)-\left(\frac{0.0571T}{J_K}\right)\right)^2}{\left(1-\coth\left(\frac{17.5J_K}{T}\right)+\left(\frac{0.0571T}{J_K}\right)\right)^2}\right) \quad (4)$$

The values of J_K and g are allowed to vary, with g constrained between 1.5 and 2.1.

The $\chi T(T)$ data of **C4MnCl** and **C6MnCl** were fit to the model from temperature T_N to 310 K. The fits are shown in Fig. 13(a) and (c), and Table 5 lists the values obtained. A value of $2J_K$ equal to −8.28(5) K and a g value of 1.96(8) were

obtained for **C4MnCl**, and $2J_K$ equal to −7.72(4) K and a g value of 1.94(6) was found for **C6MnCl**, with the negative $2J_K$ values indicating AFM interactions. Even though the *g*-factors are slightly smaller than the expected value of 2, *g*-factors smaller than 2 have been reported for related compounds in the literature.[26,30]

Eqn (5), which is used to predict the temperature at which the magnetic susceptibility has a maximum value, has also been reported:[94]

$$kT(\chi)_{max} = -1.2625(2J)S(S+1) \quad (5)$$

A very good agreement is obtained between the predicted and experimentally observed temperatures of χ_{max} for both **C4MnCl** and **C6MnCl**, as listed in Table 5.

The magnetic behaviour of the **C4MnCl** and **C6MnCl** compounds clearly indicates the presence of a magnetic phase transition(s), structural phase transition(s), or both. Detailed studies of the magnetic properties of these compounds, including FC/ZFC measurements at multiple fields, full hysteresis sweeps at multiple temperatures and low temperature X-ray diffraction studies will be required to fully understand the nature of the samples. Such measurements are in progress, but are beyond the scope of the current study.

Discussion of magnetic results

As expected, the magnetic behaviour of the two types of compounds observed in the study is markedly different due

Table 6 Summary of T_N values, $2J_K$ values, Weiss temperatures (θ) and structure classification of *n*-alkylammonium, *n*-alkyldiamonium- and arylammonium-containing perchloridomanganate hybrid perovskites reported in the literature and investigated in this study

Compound	T_N (K)	$2J_K$[a] (K)	θ (K)	RP or DJ	CSD Refcode and reference	Magnetic study reference	Year of publication of magnetic study
$(CH_3NH_3)_2[MnCl]_4$	47(3)	−10.0(2)*	—	RP	**MATCMN01**[59]	18	1972
	45.3(5)	−10.0(2)*	—		**MATCMN04**[60]	27	1979
	44	≈−8 K*	—		**MATCMN05**[61]	17	1995
	—	≈−7.25	—		**MATCMN07**[62]	32	2000
	47	—	−207.8			28	2021
	44	—	−23			99	2021
$(CH_3CH_2NH_3)_2[MnCl]_4$	43.1(2)	−9.20(5)*	—	RP	**EAMNCL**[64]	27	1979
	44	≈−8*	—		**EAMNCL11**[65]	17	1995
	—	≈−7.2	—			32	2000
	45	−8.8	—			26	2022
$(CH_3(CH_2)_2NH_3)_2[MnCl]_4$	39.2(2)	−8.90(5)*	—	RP	**PAMMNC01**[64]	27	1979
	40	≈−8*	—		**PAMMNC10**[65]	17	1995
	—	≈−7.25	—		**PAMMNC13**[8] **PAMMNC36**[66]	32	2000
$(CH_3(CH_2)_4NH_3)_2[MnCl]_4$	37	≈−8*	—	—	—	17	1995
$(CH_3(CH_2)_6NH_3)_2[MnCl]_4$	39	≈−8*	—	—	—	17	1995
$(CH_3(CH_2)_7NH_3)_2[MnCl]_4$	—	≈−7.2	—	—	—	32	2000
$(CH_3(CH_2)_8NH_3)_2[MnCl]_4$	40	≈−8*	—	—	—	17	1995
$(CH_3(CH_2)_9NH_3)_2[MnCl]_4$	—	≈−7.4	—	—	—	32	2000
$(CH_3(CH_2)_{11}NH_3)_2[MnCl]_4$	—	≈−6.25	—	—	—	32	2000
$(C_6H_5NH_3)_2[MnCl]_4$	42.6	−6.19	−126	nRP	**ZZZBMJ01**[30]	30	2021
$(C_6H_5CH_2NH_3)_2[MnCl]_4$	44.6	−7.47	−135	RP	**ZZZBMG01**[30] **ZZZBMG02**[97]	30	2021
$(C_6H_5(CH_2)_2NH_3)_2[MnCl]_4$	44.3	—	−171.4	RP	**ZZZBMD01**[29]	29	2012
	44.0	—			**ZZZBMD02–04**[98]	100	2020
	45.7	−7.65	−162			30	2021
	47	−9.9	—			26	2022
$(C_6H_5(CH_2)_3NH_3)_2[MnCl]_4$	41.8	−7.23	−148	DJ	**ZZZBMA01**[30]	30	2021
$(C_6H_5(CH_2)_4NH_3)_2[MnCl]_4$	37	—	−153.9	RP	**ZZZBLY01**[97]	7	2022
$(NH_3(CH_2)_2NH_3)[MnCl]_4$	No spin canting	−10.2	—	DJ	**ENDAMN10**[68] **ENDAMN11**[69]	26	2022
$(C_6H_5C_2H_3FNH_3)_2[MnCl]_4$	45	—	−272.67 (H⊥)[b] −273.01 (H||)[b]	RP	31	31	2022
$(HOOC(CH_2)_3NH_3)_2[MnCl]_4$ (**C4MnCl**)	47	−8.28(5)	−190(5)	nRP	This study	This study	
$(HOOC(CH_2)_5NH_3)_2[MnCl]_4$ (**C6MnCl**)	45	−7.72(4)	−175(5)	nDJ	This study	This study	

[a] Note that a negative J_K value indicates an AFM interaction, and values indicated with an asterisk are double the values reported in the original publications. [b] H⊥ indicates an applied magnetic field perpendicular to the inorganic layer, and H|| an applied magnetic field parallel to the inorganic layer.

to the difference in structures and magnetic exchange interactions.

From the parameters obtained by fitting the data of **C3MnClH$_2$O** and **C5MnClH$_2$O**, it can be deduced that the magnetic exchange along the 1D hydrogen bonded anionic chain involves very weak AFM interactions at low temperature with Weiss temperatures, θ, of −0.98(3) K and −0.83(3) K for **C3MnClH$_2$O** and **C5MnClH$_2$O**, respectively. Weak AFM exchange parameters, $2J_K$, of −0.14(2) K for both **C3MnClH$_2$O** and **C5MnClH$_2$O** are obtained, with a negative J_K value indicating AFM exchange. For these compounds the magnetic exchange pathway between Mn^{2+} ions involve hydrogen bonding interactions through coordinated water molecules and chlorido ligands, which results in very weak magnetic exchange. Magnetic coupling through a hydrogen bonding pathway was reported in a series of trinuclear and dinuclear Mn^{3+}/Fe^{3+} complexes, where weak AFM interactions exchange, with $J_K < 1$ K was reported for the Mn^{3+} complex.[95] The hydrogen bonding magnetic exchange pathway has been proposed in many studies, although the mechanism of exchange is not well understood.[96]

For the even-chain containing compounds, **C4MnCl** and **C6MnCl**, which display the 2D hybrid halide perovskite structure, a magnetic superexchange pathway involving a bridging halido ligand result in more effective magnetic exchange, with $2J_K$ values of −8.28(5) K and −7.72(4) K respectively.

The results of magnetic studies of a number of related Mn^{2+} hybrid chloride perovskites have been reported in the literature, which allows for the comparison of the results obtained in this study with the literature results. As mentioned previously, interesting magnetic phenomena are typically observed in these types of compounds, with AFM interactions observed at higher temperatures, and spin canting observed at lower temperatures. A literature survey was performed, and a number of reports on the magnetic behaviour of compounds containing *n*-alkylammonium- or aryl-ammonium cations and perchloridomanganate anions with the perovskite structure were identified, however, the magnetic behaviour of only one *n*-alkyldiammonium-containing compound has been reported. The results of the literature survey are summarised in Table 6. Information on the onset temperature of spin canting, T_N, values of magnetic exchange constants, J_K, Weiss temperatures, θ, and whether the structure can be classified as RP or DJ are tabulated. It should be noted that not all the information listed above was available for all the compounds listed in Table 6. In certain cases, the crystal structures have not been reported, hence the classification as RP or DJ could not be performed. Certain studies did not report either the magnetic exchange constant or the Weiss temperature or neither of the two. In some cases, more than one study investigated the same compound, and it should be noted that there is some variability in the values reported. In addition, year of publication of the magnetic studies are included in Table 6. It is interesting to note that there has been renewed interest in the magnetic properties of these compounds, with no less than seven magnetic studies reported in the period 2020 to 2022. Prior to that, publications on the magnetic properties of these perovskites were scant.

Since the $S = 5/2$ AFM square lattice model developed by Curély and Rouch[94] is based on a $2J_K$ Hamiltonian, and the parameter being varied is J_K, some reports in the literature give J_K instead of $2J_K$. These J_K values were multiplied by two before being included in Table 6, and are indicated by an asterisk next to the value of $2J_K$.

The $2J_K$ values in Table 6 range from −6.2 K to −10.2 K. The magnetic exchange parameter values of **C4MnCl** and **C6MnCl** of −8.28(5) K and −7.72(4) K are comparable with these values. The relatively similar $2J_K$ values are attributed to the similar superexchange Mn–Cl–Mn pathways found in both the **C4MnCl** and **C6MnCl** compounds, and related compounds in the literature. The largest $2J_K$ value of 10.2 K was reported for $(NH_3(CH_2)_2NH_3)[MnCl]_4$,[26] which is the only *n*-alkyldiammonium-containing compound listed, and the only compound exhibiting an ideal DJ structure. To determine if compounds exhibiting the ideal DJ structure generally exhibit larger magnetic exchange parameters, additional studies are required.

Considering the information in Table 6, the T_N values reported in the literature fall within the range of 37 K to 47 K. The lowest T_N values were reported for $(C_6H_5(CH_2)_4NH_3)_2[MnCl_4]$[97] and $(CH_3(CH_2)_4NH_3)_2[MnCl_4]$,[18] while the highest value was reported for $(CH_3NH_3)_2[MnCl_4]$.[18] The T_N values of **C4MnCl** and **C6MnCl** compare well with those reported in the literature, at 45.0(5) K and 43(1) K, respectively. It was reported that for $(CH_3(CH_2)_nNH_3)_2[MnCl_4]$ compounds, as the inter-layer spacing is increased, a decrease in the transition temperature, T_N, occurs.[32] However, this behaviour was seen for short chain lengths only, with $n < 4$.[32] For the longer chain lengths the change in transition temperature is independent of chain length.[32] In this current study, the slight decrease in T_N of 45.0(5) K for **C4MnCl** to 43(1) K for **C6MnCl** is probably within experimental error and therefore the transition temperature for the **C4MnCl** and **C6MnCl** is independent of cation chain length.

The only compound reported in the literature that did not display spin canting was $(NH_3(CH_2)_2NH_3)[MnCl]_4$,[26] and the authors attributed it to the fact that the compound exhibited a DJ structure, while the rest of the compounds in the family they investigated fell into the category of RP structures. It was proposed that the perfect alignment of neighbouring inorganic layers prevented spin canting. The classification of the compounds according to RP or DJ, as indicated in Table 6, indicate that all the compounds that exhibit the onset of spin canting at T_N can indeed be categorised as RP or nRP structures, except for **C6MnCl** and $(C_6H_5(CH_2)_3NH_3)_2[MnCl_4]$,[30] which are nDJ structures. Hence, it appears as if at least some degree of staggering of neighbouring inorganic layers is required for spin canting to occur, but more ideal DJ compounds should be studied to confirm this.

A very small Weiss temperature of −23 K was reported for $(CH_3NH_3)_2[MnCl_4]$ by Zhao *et al.*,[99] while Kim *et al.*[28] reported a Weiss temperature of −207.8 K for the same compound. Ignoring the Weiss temperature reported by Zhao *et al.*,[99] which seems to be an outlier, the Weiss temperatures reported in the literature fall in the range of −126 K to −273 K. The Weiss temperatures of −190(5) K for **C4MnCl** and −175(5) K for **C6MnCl** fall within this temperature range.

In summary, the magnetic behaviour of **C4MnCl** and **C6MnCl** agrees well with the magnetic behaviour of related Mn^{2+} perovskite compounds reported in the literature. This is expected, since the main difference between **C4MnCl** and **C6MnCl** and the compounds reported in the literature is the identity of the organic cation, while the inorganic portion consisting of corner sharing $[MnCl_6]^{4-}$ octahedra is similar in all the compounds. It should, however, be kept in mind that the organic cation indirectly influences the structure in that compounds containing *n*-alkyldiammonium cations exhibit DJ structures, which are not expected to show spin canting.

Conclusions

The even-odd effect is distinctly displayed by compounds comprised of *n*-carboxyalkylammonium cations and perchloridomanganate anions investigated in this study. Compounds **C4MnCl** and **C6MnCl**, containing an even number of carbon atoms, exhibit the layered 2D hybrid halide perovskite structure, with corner sharing octahedra comprising the inorganic layer, and non-interdigitated *n*-carboxyalkylammonium cations forming the organic layer. When an odd number of carbon atoms is present in the *n*-carboxyalkylammonium chain, *i.e.* compounds **C3MnClH$_2$O** and **C5MnClH$_2$O**, a 0D hybrid structure is formed, where interdigitated *n*-carboxyalkylammonium cations form the organic layer, and isolated $[MnCl_4(H_2O)_2]^{2-}$ anions the inorganic layer. This family of compounds represent a striking example of how a change in one component of a hybrid compound, in this case the addition of single carbon atom to the *n*-carboxyalkylammonium cation chain, can drastically change the type, crystal structure and dimensionality of the hybrid compound formed. Interestingly, this is only observed in the case where the metal ion is Mn^{2+}, while the 2D hybrid halide perovskite structure is always formed, regardless of the number of carbon atoms in the *n*-carboxyalkylammonium cation, for other metal ions.

The interdigitation or non-interdigitation of the cations was explained by considering the formation of a primary hydrogen bonding network comprised of the strongest hydrogen bonding donors, and whether space is available for additional hydrogen bonds to form to the primary network.

The relative orientation of consecutive inorganic layers in structures **C4MnCl** and **C6MnCl** were compared with those of related *n*-alkylammonium- and *n*-alkyldiammonium-containing hybrid halide perovskite perchloridomanganates reported in the literature, and indicated that, while *n*-alkyldiammonium-containing structures of this type always exhibit ideal DJ structures, *n*-alkylammonium-containing structures often, but not exclusively, adopt the ideal RP structure. Structures **C4MnCl** and **C6MnCl** were classified as nRP and nDJ respectively, showing the effect of a change in the cation, and the hydrogen bonding ability of the cation on the relative orientations of the inorganic layers.

It was shown through a literature survey that $[MnCl_4(H_2O)_2]^{2-}$ anions are rare, and that compounds containing 2-carboxyethylammonium or 4-carboxybutylammonium can indeed form the 2D hybrid halide perovskite structure with metal ions other than Mn^{2+}. As such, structures **C3MnClH$_2$O** and **C5MnClH$_2$O** are quite unique, in that they contain a rare anion, and do not form the 2D hybrid halide perovskite structure as was found for compounds of this type containing other metal ions.

Weak magnetic exchange between Mn^{2+} ions is observed compounds **C3MnClH$_2$O** and **C5MnClH$_2$O** which is ascribed to the fact that the exchange occurs *via* hydrogen bonding interactions in a 1D hydrogen bonded chain.

Stronger magnetic interactions are observed in compounds **C4MnCl** and **C6MnCl**, which occur *via* a halide-bridged exchange pathway. In addition, spin canting observed in compounds **C4MnCl** and **C6MnCl** is ascribed to the tilting of the octahedra in the inorganic layer. A literature survey of reports of the magnetic properties of related 2D hybrid halide perovskite compounds was conducted and highlighted the magnetic behaviour of these types of compounds. It also showed that the magnetic exchange parameters as well as spin canting onset temperatures of **C4MnCl** and **C6MnCl** correlate well with those of related compounds reported in the literature.

Conflicts of interest

There are no conflicts to declare.

Acknowledgements

The authors would like to thank Dr. F. Malan and Mr. D. Liles for assistance with crystallographic aspects. MR acknowledges financial support from the University of Pretoria, SASOL and the National Research Foundation (Grant No.: CSUR13090533011 and SRUG210427597644). SNB acknowledges financial support from SASOL and the National Research Foundation (Grant No.: 106452). MMT and CPL are grateful to the National Science Foundation (USA) for grants to purchase the SQUID magnetometer (IMR-0314773) and toward the purchase and construction of a helium recycling system (NSF DMR-1905950).

References

1 H. Do Kim, H. Ohkita, H. Benten and S. Ito, *Adv. Mater.*, 2016, **28**, 917–922.
2 A. Kojima, K. Teshima, Y. Shirai and T. Miyasaka, *J. Am. Chem. Soc.*, 2009, **131**, 6050–6051.
3 W. S. Yang, J. H. Noh, N. J. Jeon, Y. C. Kim, S. Ryu, J. Seo and S. Il Seok, *Science*, 2015, **348**, 1234–1237.

4 C. Ortiz-Cervantes, P. Carmona-Monroy and D. Solis-Ibarra, *ChemSusChem*, 2019, **12**, 1560–1575.
5 L. Mao, C. C. Stoumpos and M. G. Kanatzidis, *J. Am. Chem. Soc.*, 2019, **141**, 1171–1190.
6 Q. A. Akkerman and L. Manna, *ACS Energy Lett.*, 2020, 604–610.
7 B. Huang, P. Wang, W.-X. Zhang and X.-M. Chen, *Mater. Adv.*, 2022, **3**, 9103–9110.
8 P. Harris, F. K. Larsen, B. Lebech and N. Achiwa, *Acta Crystallogr., Sect. B: Struct. Sci.*, 1994, **50**, 676–684.
9 Y. P. Lin, L. C. Rao, M. J. Zhao, X. Y. Huang and K. Z. Du, *Dalton Trans.*, 2021, **50**, 2001–2006.
10 P. Mondal, S. K. Abdel-Aal, D. Das and S. M. Islam, *Catal. Lett.*, 2017, **147**, 2332–2339.
11 J. Li, M. Barrio, D. J. Dunstan, R. Dixey, X. Lou, J. L. Tamarit, A. E. Phillips and P. Lloveras, *Adv. Funct. Mater.*, 2021, **31**, 1–8.
12 M. Bochalya and S. Kumar, *J. Appl. Phys.*, 2020, **127**, 1–8.
13 S. Wang, X. Han, T. Kou, Y. Zhou, Y. Liang, Z. Wu, J. Huang, T. Chang, C. Peng, Q. Wei and B. Zou, *J. Mater. Chem. C*, 2021, **9**, 4895–4902.
14 G. Zhou, J. Ding, X. Jiang, J. Zhang, M. S. Molokeev, Q. Ren, J. Zhou, S. Li and X. M. Zhang, *J. Mater. Chem. C*, 2022, **10**, 2095–2102.
15 W. W. Zhong, Y. Y. Di, Y. X. Kong, D. F. Lu and J. M. Dou, *J. Chem. Thermodyn.*, 2014, **72**, 100–107.
16 S. J. Lee, M. Y. Choi and A. R. Lim, *ACS Omega*, 2021, **6**, 15392–15399.
17 S. Flandrois, N. B. Chanh, R. Duplessix, T. Maris and P. Négrier, *Phys. Status Solidi A*, 1995, **149**, 697–710.
18 W. D. van Amstel and L. J. de Jongh, *Solid State Commun.*, 1972, **11**, 1423–1429.
19 Y. Jing, Y. Yoshida, T. Komatsu and H. Kitagawa, *Angew. Chem., Int. Ed.*, 2023, 1–6.
20 B. Saparov and D. B. Mitzi, *Chem. Rev.*, 2016, **116**, 4558–4596.
21 T. Vasilchikova, V. Nalbandyan, I. Shukaev, H. J. Koo, M. H. Whangbo, A. Lozitskiy, A. Bogaychuk, V. Kuzmin, M. Tagirov, E. Vavilova, A. Vasiliev and E. Zvereva, *Phys. Rev. B*, 2020, **101**, 1–12.
22 J. B. Goodenough and A. L. Loeb, *Phys. Rev.*, 1955, **98**, 391–408.
23 J. Kanamori, *J. Phys. Chem. Solids*, 1959, **10**, 87–98.
24 G. Heger, E. Henrich and B. Kanellakopulos, *Solid State Commun.*, 1973, **12**, 1157–1165.
25 N. Achiwa, T. Matsuyama and T. Yoshinari, *Phase Transitions*, 1990, **28**, 79–97.
26 Y. Asensio, S. Marras, D. Spirito, M. Gobbi, M. Ipatov, F. Casanova, A. Mateo-Alonso, L. E. Hueso and B. Martín-García, *Adv. Funct. Mater.*, 2022, **2207988**, 1–13.
27 H. A. Groenendijk, A. J. van Duyneveldt and R. D. Willett, *Physica B+C*, 1979, **98**, 53–59.
28 Y. H. Kim and N. Hur, *J. Appl. Phys.*, 2021, **129**, 1–6.
29 S. H. Park, I. H. Oh, S. Park, Y. Park, J. H. Kim and Y. D. Huh, *Dalton Trans.*, 2012, **41**, 1237–1242.
30 L. Septiany, D. Tulip, M. Chislov, J. Baas and G. R. Blake, *Inorg. Chem.*, 2021, **60**, 15151–15158.
31 Z. Hu, L. Li, Y. Han, J. Zhang, J. Li, Z. Chen, S. Wu, Y. Zhang, H. Ye and Y. Song, *Aggregate*, 2022, 1–6.
32 K. W. Lee, C. H. Lee, C. E. Lee and J. Kang, *Phys. Rev. B: Condens. Matter Mater. Phys.*, 2000, **62**, 95–98.
33 M. Rademeyer and B. van der Westhuizen, *CrystEngComm*, 2017, **19**, 6821–6836.
34 H. Arend, K. Tichy, K. Baberschke and F. Rys, *Solid State Commun.*, 1976, **18**, 999–1003.
35 R. Boese, H. C. Weiss and D. Bläser, *Angew. Chem., Int. Ed.*, 1999, **38**, 988–992.
36 V. R. Thalladi, R. Boese and H.-C. Weiss, *Angew. Chem., Int. Ed.*, 2000, **39**, 918–922.
37 A. D. Bond, *New J. Chem.*, 2004, **28**, 104–114.
38 E. Badea, G. Della Gatta, D. D'Angelo, B. Brunetti and Z. Rečková, *J. Chem. Thermodyn.*, 2006, **38**, 1546–1552.
39 C. R. Groom and F. H. Allen, *Angew. Chem., Int. Ed.*, 2014, **53**, 662–671.
40 *Bruker, SAINT+*, Bruker AXS Inc., Madison, Wisconsin, USA.
41 G. M. Sheldrick, *SADABS*, University of Göttingen, Germany.
42 *Bruker, APEX*, Bruker AXS Inc., Madison, Wisconsin, USA.
43 *Agilent, CrysAlisPRO*, Agilent Technologies Ltd., Yarnton, Oxfordshire, England, 2014.
44 G. M. Sheldrick, *Acta Crystallogr., Sect. A: Found. Crystallogr.*, 2008, **64**, 112–122.
45 L. J. Farrugia, *J. Appl. Crystallogr.*, 2012, **45**, 849–854.
46 G. M. Sheldrick, *Acta Crystallogr., Sect. C: Struct. Chem.*, 2015, **71**, 3–8.
47 C. F. Macrae, P. R. Edgington, P. McCabe, E. Pidcock, G. P. Shields, R. Taylor, M. Towler and J. van de Streek, *J. Appl. Crystallogr.*, 2006, **39**, 453–457.
48 V. Vreshch, *J. Appl. Crystallogr.*, 2011, **44**, 219–220.
49 R. L. Carlin, *Magnetochemistry*, Springer-Verlag, Berlin, Heidelberg, Germany, 1986.
50 F. Lichtenberg, A. Herrnberger, K. Wiedenmann and J. Mannhart, *Prog. Solid State Chem.*, 2001, **29**, 1–70.
51 F. Lichtenberg, A. Herrnberger and K. Wiedenmann, *Prog. Solid State Chem.*, 2008, **36**, 253–387.
52 M. H. Tremblay, J. Bacsa, B. Zhao, F. Pulvirenti, S. Barlow and S. R. Marder, *Chem. Mater.*, 2019, **31**, 6145–6153.
53 D. B. Mitzi, *Prog. Inorg. Chem.*, 1999, **48**, 1–121.
54 M. M. Zhao, J. Z. Ge and Z. R. Qu, *Inorg. Chem. Commun.*, 2010, **13**, 1152–1155.
55 C. A. Bremner and W. T. A. Harrison, *Acta Crystallogr., Sect. E: Struct. Rep. Online*, 2003, **59**, 596–598.
56 D. M. Small, *J. Lipid Res.*, 1984, **25**, 1490–1500.
57 G. Heger, D. Mullen and K. Knorr, *Phys. Status Solidi B*, 1975, **31**, 455–462.
58 I. Mikhail, *Acta Crystallogr., Sect. B: Struct. Crystallogr. Cryst. Chem.*, 1977, **33**, 1317–1321.
59 I. Mikhail, *Acta Crystallogr., Sect. B: Struct. Crystallogr. Cryst. Chem.*, 1977, **33**, 1321–1325.
60 G. Heger, D. Mullen and K. Knorr, *Phys. Status Solidi B*, 1976, **35**, 627–637.

61 G. Chapuis, G. Brunisholz, C. Javet and R. Roulet, *Inorg. Chem.*, 1983, **22**, 455–458.
62 W. Depmeier, *Acta Crystallogr., Sect. B: Struct. Crystallogr. Cryst. Chem.*, 1976, **32**, 303–305.
63 W. Depmeier, *Acta Crystallogr., Sect. B: Struct. Crystallogr. Cryst. Chem.*, 1977, **33**, 3713–3718.
64 W. Depmeier and S. A. Mason, *Acta Crystallogr., Sect. B: Struct. Crystallogr. Cryst. Chem.*, 1978, **34**, 920–922.
65 E. R. Peterson and R. D. Willet, *J. Chem. Phys.*, 1972, **56**, 1879–1882.
66 M. Meyer, W. A. Paciorek, K. J. Schenk, G. Chapuis and W. Depmeier, *Acta Crystallogr., Sect. B: Struct. Sci.*, 1994, **50**, 333–343.
67 M. R. Ciajolo, P. Corradini and V. Pavone, *Gazz. Chim. Ital.*, 1976, **106**, 807–855.
68 K. Tichý, J. Beneš, W. Halg and A. Arend, *Acta Crystallogr., Sect. B: Struct. Crystallogr. Cryst. Chem.*, 1978, **34**, 2970–2981.
69 M. Gabro and R. A. Lalancette, *CSD Private Communication*, 2006.
70 R. D. Willett and E. F. Riedel, *Chem. Phys.*, 1975, **8**, 112–122.
71 J. C. Crowley, H. W. Dodgen and R. D. Willet, *J. Phys. Chem.*, 1982, **86**, 4046–4055.
72 K. Tichý, J. Beneš, R. Kind and H. Arend, *Acta Crystallogr., Sect. B: Struct. Crystallogr. Cryst. Chem.*, 1980, **36**, 1355–1367.
73 S. K. Abdel-Aal, *CSD Private Communication*, 2015.
74 X.-H. Lv, W.-Q. Liao, P.-F. Li, Z.-X. Wang and C.-Y. Mao, *J. Mater. Chem. C*, 2016, **4**, 1881–1885.
75 X.-H. Lv, *CSD Private Communication*, 2015.
76 T. Maris, R. Zouari, R. Duplessix, J. Leger and N. B. Chan, *PhD Thesis*, University of Bordeaux, 1996.
77 W. Depmeier and K.-H. Klaska, *Acta Crystallogr., Sect. B: Struct. Crystallogr. Cryst. Chem.*, 1980, **36**, 1065–1068.
78 R. E. Caputo and R. D. Willett, *Acta Crystallogr., Sect. B: Struct. Crystallogr. Cryst. Chem.*, 1981, **37**, 1616–1617.
79 M. Gabro and R. A. Lalancette, *CSD Private Communication*, 2006.
80 R. D. Willett, F. H. Jardine, I. Rouse, R. J. Wong, C. P. Landee and M. Numata, *Phys. Rev. B: Condens. Matter Mater. Phys.*, 1981, **24**, 5372–5381.
81 A. Kaiba, M. H. Geesi, P. Guionneau, T. A. Aljohani, L. Bih, H. Bih and S. Kassou, *J. Mol. Struct.*, 2020, **1204**, 1–19.
82 R. D. Willett, R. J. Wong and M. Numata, *Inorg. Chem.*, 1983, **22**, 3189–3194.
83 L. Efimenko, I. A. Churakov, A. V. Ivanova, N. A. Erofeeva and O. S. Demina, *Zh. Neorg. Khim.*, 2017, **62**, 1476–1478.
84 H. Hillebrecht, *CSD Private Communication*, 2020.
85 M. Krummer, B. Zimmermann, P. Klingenberg, M. Daub and H. Hillebrecht, *Eur. J. Inorg. Chem.*, 2020, 4581–4592.
86 W. Yang, X. Xiao, H. He, G. Tong, J. Hu, X. Xiao, J. Chen, M. Li and Y. He, *Cryst. Growth Des.*, 2021, **21**(10), 5731–5739.
87 L. Li, *CSD Private Communication*, 2020.
88 M. C. Etter, *Acc. Chem. Res.*, 1990, **23**, 120–126.
89 X. Li, J. M. Hoffman and M. G. Kanatzidis, *Chem. Rev.*, 2021, **121**, 2230–2291.
90 R. Dingle, M. E. Lines and S. L. Holt, *Phys. Rev.*, 1969, **187**, 643–648.
91 B. Huang, P. Wang, W.-X. Zhang and X.-M. Chen, *Mater. Adv.*, 2022, **3**, 9103–9110.
92 I. Dzyaloshinsky, *J. Phys. Chem. Solids*, 1958, **4**, 241–255.
93 L. J. De Jongh and A. R. Miedema, *Adv. Phys.*, 2001, **50**, 947–1170.
94 J. Curély and J. Rouch, *Phys. B*, 1998, **254**, 298–321.
95 I. Nemec, R. Herchel, T. Šilha and Z. Trávníček, *Dalton Trans.*, 2014, **43**, 15602–15616.
96 V. Zeleňák, A. Orendáčová, I. Cısařová, J. Černák, O. V. Kravchyna, J.-H. Park, M. Orendáč, A. G. Anders, A. Feher and M. W. Meisel, *Inorg. Chem.*, 2006, **45**, 1774–1782.
97 S. He, S. Hao, J. Lin, N. Wang, J. Cao, Z. Guo, C. Wolverton, J. Zhao and Q. Liu, *Inorg. Chem.*, 2022, 11973–11980.
98 M. E. Kamminga, R. Hidayat, J. Baas, G. R. Blake and T. T. M. Palstra, *APL Mater.*, 2018, 66106.
99 H. Zhao, H. Fu, Z. Hu, Q. Fu, H. Tao, J. Weng, L. Xiong and Z. Cheng, *CrystEngComm*, 2021, **23**, 5208–5213.
100 K.-Y. Kim, G. Park, J. Cho, J. Kim, J.-S. Kim, J. Jung, K. Park, C.-Y. You and I.-H. Oh, *Small*, 2020, **16**, 1–12.